Materials Innovations

HΣXA Publishers

Photocatalytic Materials | Review Article | http://doi.org/10.54738/MI.2022.2901

# Recent Innovations in Low Dimensional ZnO Nanostructures/Nanocomposites for Photocatalytic Degradation

**Maryam Basit[1], Sofia Javed[1]*, Saqib Ali[1], Akbar Ali Qureshi[1], Iftikhar Hussain Gul[1], Muhammad Aftab Akram[1]**

**1** School of Chemistry & Materials Engineering, National University of Science and Technology, H-12, Islamabad, 44000, Pakistan

OPEN ACCESS

This article is part of online collection of special issue on "Women in Materials Science"

**Received:** 05 June 2022

**Accepted:** 07 August 2022

**Published:** 28 September 2022

**Citation:** Basit M, Javed S, Ali S, Qureshi AA, Gul IH, Akram MA (**2022**) Recent Innovations in Low Dimensional ZnO Nanostructures/Nanocomposites for Photocatalytic Degradation. *Materials Innovations 2* (9), 225-254.

***Correspondence**: (Sofia Javed) s.j@nust.edu.pk



Published By Hexa Publishers

**ISSN**
Electronic: 2790-1963

*The energy and environmental application of materials can be improved dramatically by efficiently consuming a large section of the solar spectrum. Scientists are exploring the wide band gap metal oxides and their nanocomposites as heterogeneous photocatalysts for effective performance in solar wavelengths. Increased surface area, efficient photon absorption, and reduced recombination rate can be achieved by structural engineering and developing efficient nanocomposites. A thorough review of recent innovations in ZnO nanostructures/nanocomposites exclusively for photocatalytic dye degradation has been conducted. The review provides insight into the effects of ZnO nanostructure and recent advancements in ZnO nanocomposites to improve the photocatalytic activity of organic pollutants under different radiations. The review concludes that structural and material engineering can boost the photocatalytic performance of ZnO structures.*

**Keywords:** ZnO nanostructures, Photocatalytic degradation, ZnO nanocomposites

## INTRODUCTION

In the present era of industrial development and modern civilization, the rising pollution level and poor water management have contaminated natural water reservoirs. Lack of pure water has affected the living standards. The essential requirement for drinkable water has increased alarmingly in underdeveloped countries[1]. Ensuring the availability of healthy water and ecological water management is a huge concern. Sustainable Development Goals (SDGs) seven is majorly defining the parameters of clean and drinkable water set by the United Nations (UN)[2]. The reclamation of wastewater is one of the attractive solutions. The excess use of synthetic products in daily life has built up the verity of persistent organic pollutants (POPs). The POPs are long polymer chains resilient to common water treatments. The complex composition, persistent nature, and detrimental effects of these pollutants have made them difficult to remove during conventional water treatments[3,4]. Such pollutants can inculcate through generations and cause many life-threatening damages[5]. Scientists and researchers are working to resolve this issue by employing different procedures.

Various water treatments have been developed to remove such pollutants by ionizing radiations[6], metal-organic frameworks (MOF)[7], electrochemical activation of persulfates compounds[8], biodegradation/bioremediation[9], electrocoagulation[10], ultrasonic treatment[11] and many more. These methods mainly focus on removing the POPs from liquid; however, the byproducts are in the solid phase[11–14], which requires advanced oxidation processes (AOPs) for further treatment[15–17]. The high production rate of POPs, costly wastewater treatment reactors and high energy consumption to break down the organic pollutants are major obstacles[18–20]. These issues must be addressed in a single solution. One of the efficient and practical solutions is photocatalysis, as it utilizes the most extensively available natural resource of sunlight rather than any external sources of energy, which reduce the cost of the reclamation. Moreover, it is environmentally friendly. Photocatalyst is reported to be highly effective for the degradation of organic pollutants[21–27], generation of hydrogen fuel[28], antibacterial activity[29,30], and air purification[31]. The catalytic effects are more pronounced at the nano level due to the change in bond polarization, the shift in the adsorbent range of wavelength, increased surface area, and increased reaction site available for redox reaction as compared to the bulk material[32,33].

Numerous material scientists are investigating fabricating highly photoactive materials for water purification applications. The two classes of photocatalysts are homogeneous and heterogeneous catalysts. Homogeneous photocatalysis is a mixture of hydrogen peroxide and $Fe^{2+}$ based salt commonly known as Fenton's reagent. It produces hydroxyl radical when exposed to UV light, wavelength above 300 nm[34]. Whereas heterogeneous photocatalysts are semiconductor oxides, which degrade the organic pollutes at relatively longer wavelengths[35]. $TiO_2$ is extensively studied for photocatalytic application. $TiO_2$ has got attention due to its low-cost production, chemically inert nature, and compelling photo activity degradation of organic pollutants such as water-soluble pesticides[36], antibiotic erythromycin[37], dinitrophenol (DNP)[38], organic material with the nitrogen-based functional group[39], xenobiotic organic pollutants[40], volatile organic compounds[41,42], saturated and aromatic hydrocarbons[43–45], $TiO_2$ has also been used to assist the conversion of aromatic pollutants in fuels[46] and non-biodegradable azo dyes[47–49] with a UV light source. The limitation of $TiO_2$ is its wide bandgap (3.2 eV) and low quantum efficiency[50]. Many attempts are made to improve the photocatalytic efficiency by doping metals[51–55] and non-metals[56,57], synthesis of nanocomposite[58–61] and surface alterations[62–65]. In contrast to $TiO_2$, ZnO is not well studied in photocatalytic activity[66].

ZnO can be a promising entrant with its numerous morphologies, high stability, mechanical strength, high bulk of electron mobility, higher absorption coefficient, a wide bandgap relatable to $TiO_2$, and nontoxicity[66]. Summary of structure and properties of ZnO is given in Table 1. This review is about the detailed study of morphological effects of ZnO over photocatalytic activity to increase its practical application in this field, in the perspective of the recent development of ZnO-based materials in water treatment under ultra-violate and visible ranges. Moreover, this review will develop insight into the prospects and future challenges to exploiting ZnO for water purification applications and enable researchers to improve the efficiency and effectiveness of ZnO-based photocatalyst.

## PHOTOCATALYTIC MECHANISM OF ZnO

The photocatalytic activity is mainly dependent on incident wavelength and catalyst bandgap energy. Semiconductors are mostly used as sensitizers, the exposure to light stimulates the redox reaction because of the electronic band structure[67,68].

The step by step explanation of ZnO photocatalytic activity are as follows[69]:

1. If the incident photon energy is equivalent to, or higher than the bandgap of the ZnO causes the electrons in the valance band jump to the conduction band.

2. Leaving behind the holes in the valance band, which oxidize the donor molecule and react with a water molecule to produce hydroxyl radicals ($OH^-$).

3. The electron in the conduction band forms a superoxide oxygen ion (O*). Ion undergoes a reduction reaction to form water. The redox reaction on the surface of the ZnO photocatalyst degrades organic pollutants and gives green products.

$ZnO + h\nu \longrightarrow ZnO\ (e^-_{(CB)}) + (h^+_{(VB)})$

$ZnO\ (h^+_{(VB)}) + H_2O \longrightarrow ZnO + H^+ + OH^*$

$ZnO\ (h^+_{(VB)}) + OH^- \longrightarrow ZnO + OH^*$

$ZnO\ (e^-_{(CB)}) + O_2 \longrightarrow ZnO + O_2{}^{*-}$

$O_2{}^{*-} + H^+ \longrightarrow HO_2{}^*$

$HO_2{}^* + HO_2{}^* \longrightarrow H_2O_2 + O_2$

$ZnO\ (e^-_{(CB)}) + H_2O_2 \longrightarrow OH^* + OH^-$

$H_2O_2 + O_2{}^{*-} \longrightarrow OH^* + OH^- + O_2$

$H_2O_2 + h\nu \longrightarrow 2OH^*$

Organic pollutants + $OH^* \longrightarrow$ Intermediates

Intermediates $\longrightarrow CO_2 + H_2O$

ZnO absorbed photons of energies equitant or higher than the bandgap. The electrons in the valance band get excited and jump to the conduction band, leaving positively charged holes in the valance band. The photon induces the exitron pair to emerge to the surface of the ZnO nanostructure and initiate the redox reaction. Hydron reacts with water and produces $OH^-$ radicals. Electrons react with oxygen

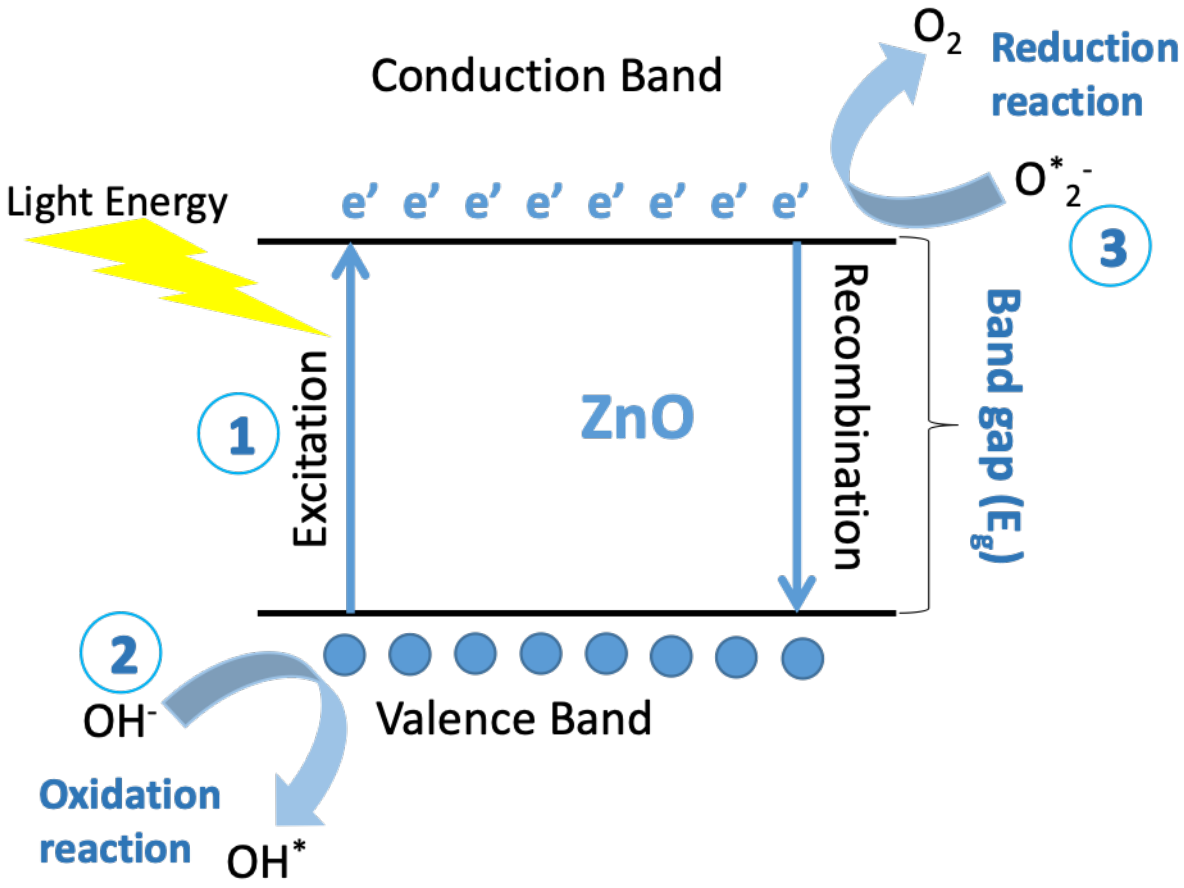


*Figure 1. Schematic representation of ZnO photocatalytic mechanism.*

by giving superoxide anion and later react to hydrogen peroxide to give out hydroxyl radical. These $OH^-$ radicals interact with organic pollutants on the surface of ZnO to degrade them to intermediates and then to $CO_2$, $H_2O$, and other green products [70–72].

## WHY ZnO AS PHOTOCATALYST?

The major parameters determining the photocatalytic activity are crystal structure, shape, size, and active surface area of the catalyst. Moreover, reaction temperature, pH levels, light intensity, amount of photocatalyst and concentration of pollutants in water are controlling factors of the activity [71,73,74]. ZnO is an II-VI compound n-type semiconductor with a direct wide bandgap of 3.37 eV. ZnO has high excitation energy of 60 meV and a higher absorption coefficient at ambient temperature than $TiO_2$. Moreover, various ZnO morphologies can easily attain anisotropic growth relative to the other semiconductor materials. The crystallized site is photoactive at UV and visible wavelengths and produces rapid electron-hole pairs [75]. The Wurtzite crystal structure of ZnO, controllable shape, size, and number of active sites at nano levels makes ZnO an efficacious contender for photocatalytic studies [74]. However, the recombination rate is yet to control to increase efficiency. The cost of ZnO production is 75% lower than the $TiO_2$ and $Al_2O_3$ nanoparticles (NPs) [76]. Additionally, the mechanical [77], electrical and optical properties [78] of ZnO are very supportive for the photocatalytic application [71,74]. The surface area increase, along with the polar faces, due to its unique P63mc space group of ZnO. $Zn^{+2}$ ions and $O^{-2}$ ions are linked via two connecting tetrahedral lattices, which increases the polar symmetry in the c-axis resulting in piezoelectricity and spontaneous polarization of ZnO nanostructures, specifically two-dimension (2D) nanosheets and thin films [79], which makes them effective photocatalysts. The large surface-to-volume ratio, numerous active sites and large surface area enable a larger number of contaminants to attach to hydroxyl radical. Hence the degradation rate can be increased effectively.

*Table 1. General overview of characteristics of ZnO.*

| | | | |
|---|---|---|---|
| **Colour** | White powder | Dielectric constant | 10.53 |
| **Crystal structure** | Wurtzite | Piezoelectric Modulus (d33) | 1.28562 C/m$^2$ |
| **a=b (lattice constant)** | 3.25 A° | Poisson's Ratio | 0.36 |
| **c (lattice constant)** | 5.2 A° | Elastic Anisotropy | 0.13 |
| **c/a** | 1.6 | Bulk Modulus | 130 GPa |
| **Band gap in bulk (Eg)** | 3.37 eV | Shear Modulus | 41 GPa |
| **Band Gap (direct)** | 0.732 eV | Space Group | $P6_3mc$ |
| **Binding energy** | 60 MeV | Zn-O bond length | 1.89 Å |
| **Formation Energy / Atom** | -1.799 eV | Cp (specific heat) | 0.497 (J/g K) |
| **Density** | 5.44 g/cm$^3$ | Melting point | 1975 K |
| **Refractive Index n** | 2.32 | Debye Temperature | 416 K |

In the discussion below, the morphological effect of ZnO will be studied in detail with the improvement perspectives.

## ZnO MORPHOLOGIES

The division between nanostructures is based on the total number of dimensions in the nanoscale. Nanorods, nanowires, nanotubes, nanoneedles and nanofibers are included in one-dimension (1D) nanostructures. Nanosheets (NSs) and thin films come under the umbrella of two-dimension (2D), and nanoflowers are covered in three-dimension (3D) nanostructures. Quantum dots (QDs) and nanoparticles (NPs) are zero-dimension (0D) nanostructures because all three dimensions are in the nanoscale[80]. The quantum confinement effects are very pronounced at nanoscales. QDs arrays, elongated arrays, planar arrays and ordered structures are a division of nanostructures in the perspective of quantum effects. Morphologies of ZnO are vital for their use in different applications majorly, including photovoltaics and photocatalysis. The attractive attributes of ZnO nanostructures are high electron mobility and high mechanical strength. Chemical stability and non-toxicity are the researcher's reasons for increasing curiosity about ZnO for different practical applications[81,82].

ZnO thin film transmission is increasing to 75%, and the bandgap is tailored from 3.17eV to 2.79 eV with doping of Co transition metal ion[83]. The tailored bandgap and transmission make ZnO a good candidate for photovoltaic, higher frequencies device operation[84], optoelectronics[85] and conductive film application[83] . ZnO QDs and nanowires are used for cancer diagnostics and treatment due to their sustainability, biocompatibility, high isoelectric point, and tunable morphologies[86]. The unique feature of ZnO nanowires is molecular identification, mechanical strength, the flexibility of ZnO nanorods, and their sensitivity to different gases[87], and ultraviolet light enables them for sensing application[88,89]. ZnO nanowires are grown aramid fabrics that enhance impact resistance[90,91], which makes them a potential candidate for soft body armour in defence and sports fields.

### Zero-dimensional ZnO

The largest active surface area, higher quantum yield and stability of ZnO QDs and NPs make them attractive for photocatalyst application[79]. A larger number of organic pollutants can absorb onto NPs and QDs surfaces. Resulting in rapid degradation sites for the organic pollutant.

#### *Quantum dots*

The large number of polar facets in ZnO QDs and increases reactive sites make them an effective option for photocatalyst. The availability of a controllable bandgap for the photoactive redox reaction and the high surface-to-volume ratio have opened new vistas for research.

ZnO QDs prepared by the modified wet chemical method by Mohamed, W.A. et al., The reported crystalline size is 2.9 nm with a tailored band gap of 3.57 eV and a surface area of 312.1 m$^2$/g. The profound blue shift is observed in observation peek at 315 nm and fluoresce spectra shifted to 500 nm due to the decrease in crystallized size and prominent quantum confinement. The ZnO QDs show 25% decay of Coomassie Brilliant Blue R (CBBR) dye in 330 minutes under sunlight irradiation. After nine cycles, the photocatalytic activity is not significantly affected[92]. However, the low degradability has argued the researchers to develop an advanced technique by tailoring the ZnO bandgap.

Doping is an effective technique to tailor a bandgap within semiconductors. Sowik, J., et al., modified ZnO QDs bandgap doping lanthanides (Eu, Er, Tb, Yb, Ho and La) metals. Rarer earth metal doped ZnO QDs (ZnO/RE) are synthesized by the sol-gel method. ZnO/La is reported to increase the quantum yield to 81%. ZnO/Er shows exceptional photocatalytic removal of phenol up to 90% in an hour under UV-Visible light. ZnO/La is showing lower values of fluorescence and PL intensities rele-

vant to pristine ZnO QDs. The maximum absorbance is reported at 340 nm. The lattice constant "a" almost remain almost unchanged, whereas "c" varies with doping of different rarer earth metals from 5.179 to 5.198 (A°). The effective increase in photocatalytic activity is observed in ZnO/Er due to the additional electronic state 3d/4f introduced by $Er^{+3}$ rare earth metals ion in the bandgap of ZnO QDs. Which increase the absorption spectrum, assist exciton excitation and reduce the recombination rate[93]. The introduced defects by doping majorly different ionic radii and excessive stress within crystal lattice are responsible for the weak Zn-O bonding. It directly influences the optical properties and quantum yield of the doped ZnO QDs. The high cost and lack of availability of rare earth metals are limiting factors for their extensive use.

The hybrid formation is a new strategy to exploit two effective materials for an application. CuO is an extensively used heterogeneous photocatalyst[95–97]. Fakhri, A., et al., combined both the CuO and ZnO effectively. CuO NSs decorated by ZnO QDs by the hydrothermal method. The crystalline size of CuO NSs has reduced drastically from 12.5 nm to 3.2 nm along with the reduction of the bandgap from 2.01 eV to 1.86 eV by adding ZnO QDs to CuO NSs. Upon the irradiation of sunlight and UV light, tetanus toxin (TeNT) decays up to 75%[98]. The effective hybrid (ZnO QDs/CuO NSs) formation is due to the coupling of CuO NSs, and ZnO QDs enhanced the photoactivity. Moreover, the active surface area available for the organic pollutant is increased along with the reduced recombination rate of the charges. However, the dose of pollutant used for the study as the model is very low (in Table 2)., which does not encourage the trade use of ZnO QDs/CuO NSs hybrid.

Vattikuti, S.P., et al., synthesized hybrids photocatalyst. $ZnO/SnO_2$ QDs (SZ) are deposited on graphitic carbon nitride nanosheets (g-$C_3N_4$) by the in-situ co-pyrolysis method. The photocatalyst reported being active in visible light and effective for producing hydrogen fuel applications. The surface area of SZ/g-$C_3N_4$ hybrid has almost doubled to 46.38 $m^2\ g^{-1}$ from 24.7 $m^2\ g^{-1}$. The pore size is also increased to 0.234 $cm^3\ g^{-1}$, which is one of the major factors in increasing the efficiency due to the increase in the active site. The bandgap of hybrid lies in the visible range, i.e., 2.75 eV. The SAED pattern ant HRTEM image clearly indicate ZnO and coating $SnO_2$ (in Figure 2 (a and b)) and The Rhodamine B (RhB) dye is 99% degraded under visible light in 60 minutes (in Figure 2 (c)). During four cycles, the photocatalyst remains stable and keeps up its performance[94]. The hybrid structure shows outstanding results because of the synergic effect, rapid electron mobility, bandgap tailoring, reduction in recombination rates, the larger number of active sites and increased surface area. The in-situ growth enables better interfacial strength and random dispersion of $ZnO/SnO_2$ QDs over the NSs. The approach to designing an SZ/g-$C_3N_4$ hybrid is very appealing further research is required to see the response to different organic pollutants at different pH, temperature, wavelength, and other influencing factors to the performance.

Kumar, K.A., et al., synthesized heterojunction of ZnO QDs with reduced graphene oxide (rGO). ZnO QDs are prepared by simple chemical precipitation, and rGO is prepared by in situ hydrothermal methods. The clears placement ZnO QDs over rGO can be seen in TEM images (in Figure 3 (a and b)) Crystalline size of hybrid is reduced to 3.2 nm along with the reduction in band gap to 2.1 eV. Increase in surface area from 60 $m^2\ g^{-1}$ to 135 $m^2\ g^{-1}$, whereas the size of the pores reduces from 43.1 Å to 37.9 Å, escalating the hybrid photocatalyst's efficiency. The heterojunction is exploited for the degradation of tetracycline (TC) and hexavalent chromium (Cr (VI)). The heterojunction is active in the visible range for 120 min. It degrades tetracycline (TC) and hexavalent chromium (Cr (VI)) pollutants up to 68% and 84% respectively (in Figure 3 (c))[99]. The excited electron can move along the surface of rGO, which reduces the recombination of excitons. The electron on the surface of rGO is widely available to the organic pollutants for photodegradation. The time required for redox reaction is a limiting factor for the high performance of photoactive decay by the ZnO/rGO heterojunction.

Wang, X. and J.J.O.M. Li, prepared ZnO QDs coated with Ag by facile sol-gel method. Ag coated ZnO QDs are reported to be photoactive under artificial sunlight. The performance is 99% in 80 min to minimalize methylene blue (M.B). The crystalline size of 11.86 nm of ZnO/Ag. Ag coating of approximately 0.37 nm was done on the ZnO QDs Bandgap energy drops to 2.92eV at point B in figure 4a from 3.38 eV at point A. Density functional theory calculations indicate that further decrease can be achieved to 1.744 eV by increasing surface defects (in Figure 4(b and c)). The designed photocatalyst exhibits stable nature after three successive cycles of photodegradation[100] Ag does not cover the ZnO Q.D.s completely. The impartial coating developed the easy flow of exitron during the redox reaction. The band tailoring, reduction in the recombination rate and surface plasmon resonance by imperial coating Ag atoms has significantly enhanced the performance of the nanocomposite. However, an enormous amount of photocatalyst (in Table 2) is used for photodegradation of M.B., Which is not practically supportive for the frequent use in water purification applications.

Fakhri, A. et al., decorated CuO NSs with ZnO QDs. Photocatalyst is reported to be effective in UV light for the degradation of 1-methyl-4-phenyl-1,2,3,6-tetrahydropyridine (MPTP) and Tetanus toxin (TeNT). In 60 minutes, the toxins are degraded up to 80% in

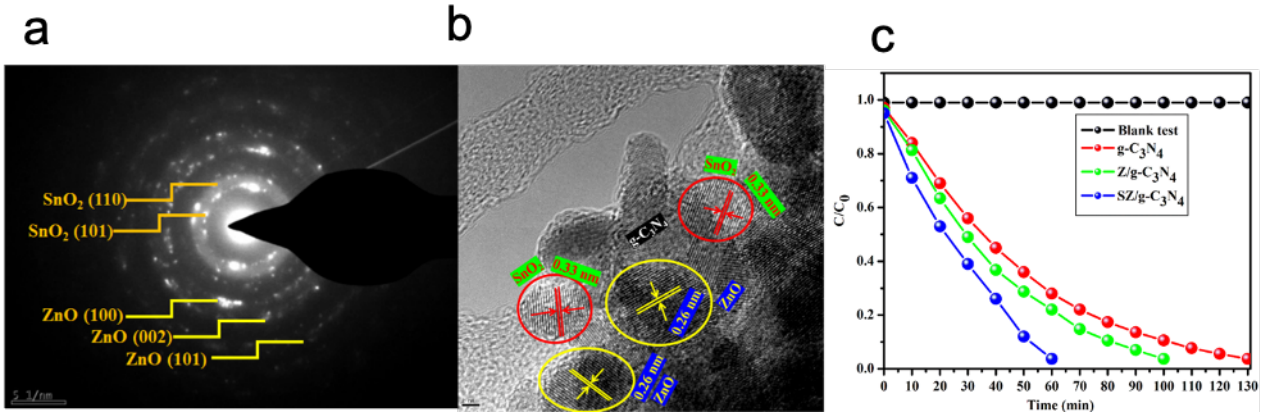


*Figure 2. (a) SAED pattern of the SZ/g-$C_3N_4$ catalyst. (b) HRTEM image and (c) Photocatalytic activities of different photocatalysts for the degradation of RhB under visible light irradiation*[94]*. Reprinted with permission from ref. 1*

UV and 75% in UV with the assistance of a microwave. The hydrothermal method prepared the ZnO QDs/CuO NSs with a crystallite size of 3.2 nm. The bandgap is significantly reduced to 1.86 eV with an absorption spectrum in the green region. The photocatalyst was stable for ten consecutive cycles. The operational temperature range between 70 to 320°C for photocatalytic reaction. The MPTP and TeNT solution was introduced to the wastewater reactor at 250 °C[101]. Due to the high redox reaction temperatures, ZnO QDs/CuO NSs photocatalyst is unsuitable for extensive use.

Iqbal, A. et al., ZnO QDs adsorbed on $TiO_2$ anatase by sol-gel assisted hydrothermal method. The highly porous ZnO QDs/$TiO_2$ nanocomposite with an average crystalline size of 9.22 nm with an average pore size of 510 nm. The induced oxygen vacancies and surface defects indicate the quantum confinement effect. Bandgap was 3.24 eV, relatively less than ZnO. The catalyst is used for the breakdown of tetracycline (TC). It is effective under fluoresce light. TC is degraded up to 98% in 90 minutes. The effenciay is not significantly effective after four cycles[103]. High energy excitons are produced due to the quantum confinement effect. The z-scheme heterojunction delay recombination of charges. The large active surface area and high quantum confinement effect enable the ZnO QDs/TiO2 nanocomposite for photocatalytic activity. Nevertheless, the sensitivity to a specific wavelength of fluoresce-light limits its practical use.

Zhou, Q., et al., reported ZnO QDs decorated $ZrO_2$-$TiO_2$ hollow spheres for degradation of Congo red (CR) up to 94% in 120 minutes under UV, visible light, and simulated sunlight. ZnO QDs@$ZrO_2$–$TiO_2$ is prepared using a sol-gel and colloidal template method. the SEM and HR-TEM images vividly exhibits the morphology and phase of all the components of the hybrid (in Figure 5 (a-c)). The bandgap is reported in the visible range of 2.95eV, less than both $TiO_2$ and ZnO. The surface area increases 46.14 $m^2$ $g^{-1}$ with pores size of 13.39 nm. The average crystalline size was reduced to 15.78 nm from 16.5 nm. Photocatalytic efficiency reduces by 10% in three consecutive cycles[102]. The two junctions are developed. One is between anatase and rutile $TiO_2$, another junction between $TiO_2$ and $ZrO_2$ along with synergic effects between ZnO QDs and $ZrO_2$. The structure has both homojunction and heterojunction, which are highly effective for photocatalytic activity. however continuous decrease in the effenciay of the photocatalyst is encouraging for the commercial preparation.

ZnO QDs have a high surface-to-volume ratio, and a pronounced quantum confinement effect makes them a good candidate for photocatalytic application. The larger surface area allows larger numbers of pollutants to react at the surface of ZnO QDs. Their combination with different elements such as doping, hybrid and heterojunction formation allows researchers to tailor bandgap and reduce recombination rate significantly. The introducing stresses in the crystal structure of ZnO QDs shift the absorbance wavelength, which shifts the photoactive response to the visible range. Moreover, the hybrid with other nanostructures enhances the system's synergic effects and charge mobility. The interfacial effects within nano junctions and hybrid develop better charge separation. Excited charges are available for a longer time to react with organic pollutants.

### *Nanoparticles*

Many studies investigate the role of ZnO NPs in photocatalytic activity to decompose organic pollutants. The surface-to-volume ratio and availability of active sites are majorly affecting the catalytic efficiency.

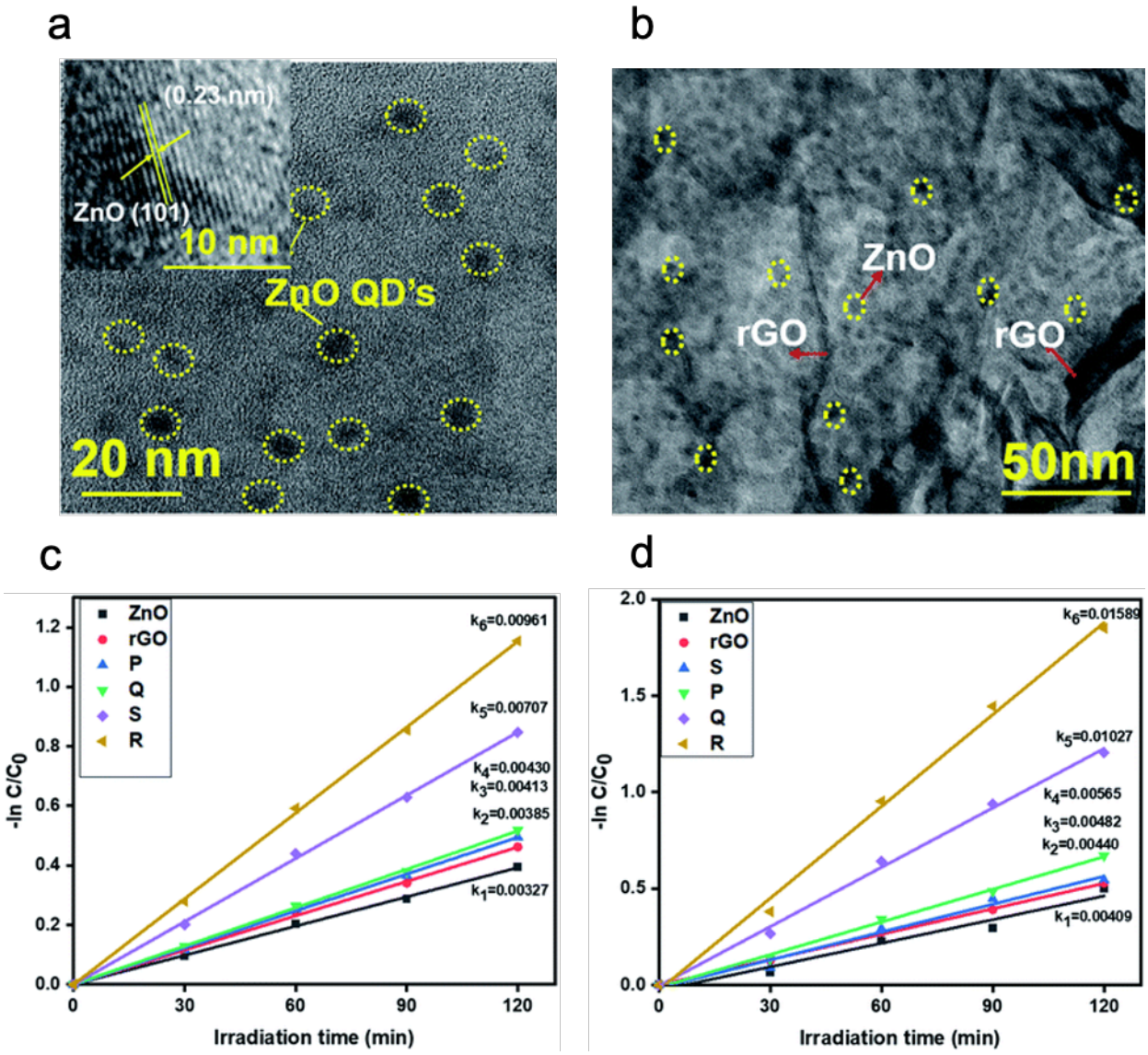


*Figure 3. (a) TEM images of ZnO (inset: lattice fringes of ZnO), (b) ZnO/rGO composite, (c) Photodegradation TC and (d) Cr(VI) by ZnO, rGO and ZnO/rGO[99]. Reprinted with permission from ref. 2*

Mahdavi, R. and S.S.A.J.U.S. Talesh synthesized ZnO NPs by the sol-gel method. ZnO NPs are exposed to ultrasonic waves. Later, ZnO N.P.s are used to study photocatalytic degradation of methyl orange (MO) under the radiation of ultraviolet light up to 98% in 180 mins. MO degradation rate increases, whereas crystal and particle size decrease with an increase in power and time of exposure to ultrasonic waves. Untreated samples are not as effective as ultrasound-treated samples[104]. The increase in efficacy is due to the rapid shift of localized pressure within the reacting chamber. The surface atoms of ZnO N.P.s are weakly linked to the main lattice structure. The excess energy provided to these atoms will contribute to the availability of active, reactive sites. The redox reaction sensitivity to the visible light is archived, but the long exposure time for the azo dye to photodegrade urges the scientist for further research.

Ghaderi, A. et al., MO is also removed up to 99% in just 35 minutes $ZnO/SnO_2$ hybrid synthesized by sol-gel method. The weight percentage of $SnO_2$ is directly proportional to the time of incident UV light and performance (in Figure 6 (a and b)). 99% MO decay under UV light in 35 mins. The bandgap was reduced to 3.25 eV compared to the bulk due to the size reduction of ZnO nano levels[105,106]. The $ZnO/SnO_2$ hybrid's compound effect increases the rate of redox reaction

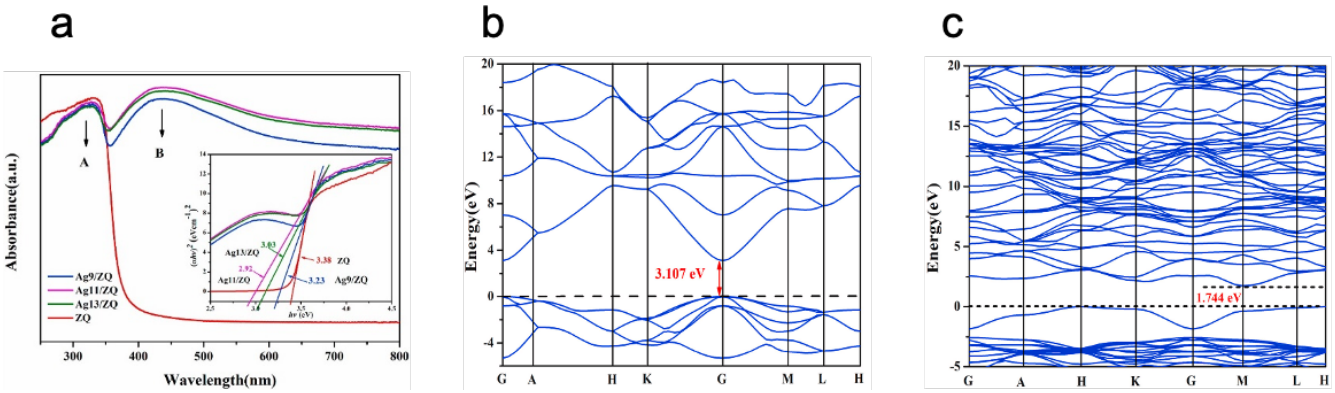


*Figure 4. UV–vis absorption spectra of Ag coated ZnO QDs (inset: Tauc plots).,* ***(b)*** *DFT Calculated band structures of defect-free ZnO, and* ***(c)*** *ZnO with introduced surface defects*[100]*. Reprinted with permission from ref. 3*

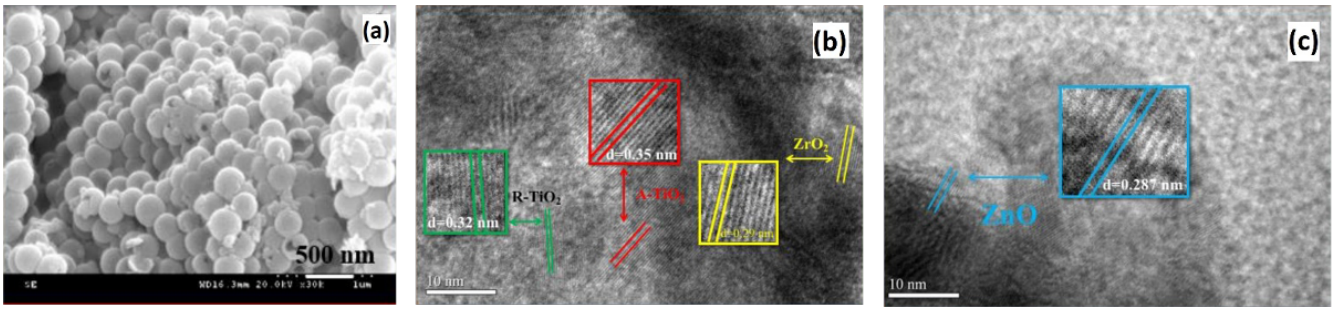


*Figure 5. (a) SEM images of 0.5 ZnO QDs@$ZrO_2$–$TiO_2$, (b) HR-TEM images of 0.5 ZnO QDs@$ZrO_2$–$TiO_2$ (c) Enlarged image of the selected area*[102]*. Reprinted with permission from ref. 4*

due to the excessive exciton excitation. The availability of free charges enhances the release of hydroxyl radicals, hence the photocatalytic activity increase. Only sensitive to UV-light is a limiting factor for the extensive use of $ZnO/SnO_2$ hybrid for water treatments.

Mahdavi, R. and S.S.A.J.A.P.T. Talesh, synthesized Al-doped ZnO by sol-gel method. The crystal size is 10 nm of Al-ZnO photocatalyst. MO is degraded under U.V. light up to 65% degradation after 180 minutes. The band gap decreases to 2.93 eV; however, the absorbance wavelength increases to 370 nm relative to the pure ZnO NPs. An interesting fact is that the increase in doping %age of Al changes the morphology and crystal size (in Figure 7 (a-f))[107]. The vivid shift in morphologies is due to the addition of $Al^{+3}$ charges replacing $Zn^{+2}$ in the crystal lattice. At higher weight %age of Al doping, the planer defect increase. The intrinsic polarity of nanostructure causes surface energy to quick anisotropic growth in some other direction; hence the nanostructure changed from nanospheres to nanorods. The change in morphology eventually influences the performance of the photocatalyst.

Zhang, X. et al., made another effort with Al-doped ZnO NPs. 99% of MO is degraded in 30 minutes under UV light. Al-ZnO photocatalyst was prepared by the sol-gel combustion method with a crystallite size of 6.4 nm and a band gap of 3.23 eV[108]. The increase in photocatalytic activity is due to the reduction in particle size, increase in the surface area and availability of excess hydroxyl ions for MO degradation. Despite the high performance, Al doping is not suggested to be utilized commercially because the study above used enormous amount of photocatalyst for water purification (in Table 2).

Carbon has outstanding properties which push researchers to investigate them for different applications. The carbon-based nanostructures are exploited in water purification systems as well. Low cost and easy availability are the factors which increase the interest in carbon materials[109]. Liang, H., et al., prepared the visible light active catalyst by L-CQDs/ZnO hybrid. The steaming ammonia and hydrothermal method are used to create a hybrid. The ZnO NPs particle size range between 10 to 40 nm and L-CQDs 1-3 nm. The bandgap of the hybrid is 2.69 eV. Phenol is degraded as a model pollutant, up to 99% in 5 hours. Moreover, the photocatalyst was used for

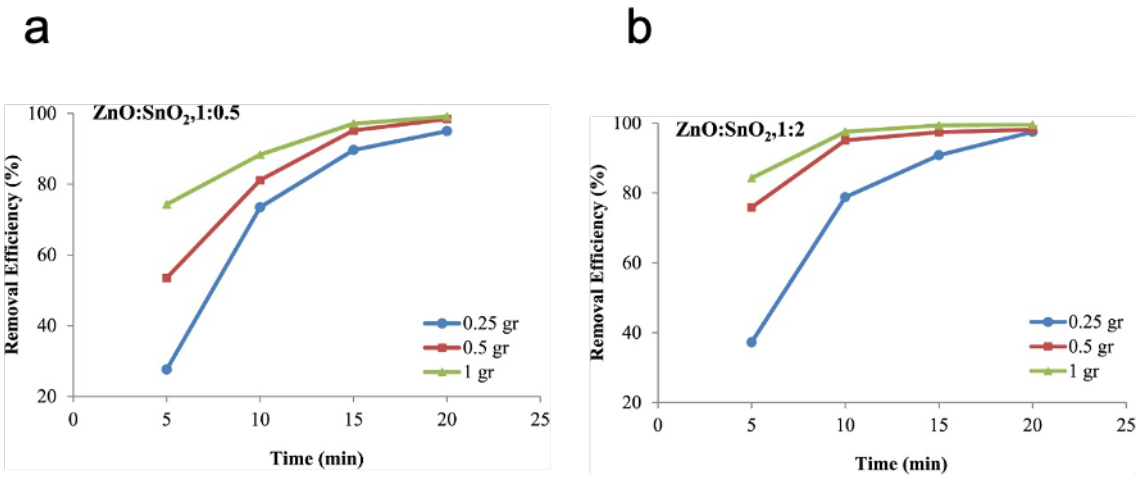


*Figure 6. (a) Photocatalytic degradation of MO in ZnO: $SnO_2$,1:0.5 hybrid, influence of concentration, (b) Photocatalytic degradation of MO in ZnO: $SnO_2$,1:2 hybrid, influence of concentration*[105]*. Reprinted with permission from ref. 5*

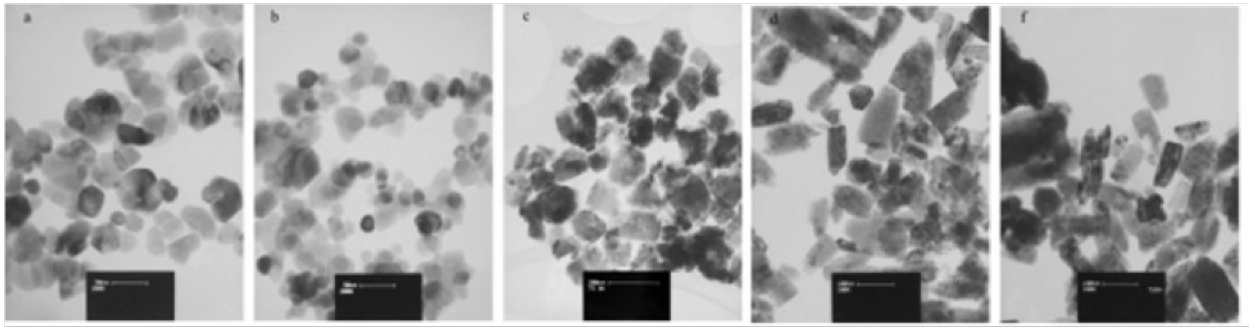

*Figure 7. TEM images of (a) ZnO, (b) Al-ZnO 1%, (c) Al-ZnO 3%, (d) Al-ZnO 5% and (f) Al-ZnO 7%*[107]*.*

up to 10 cycles without any major decrease in efficiency[110]. The increase in photocatalytic activity is due to the bandgap compatibility of ZnO and L-CQDs. The charge transfer enhanced the absorption to the visible range. Further research is still required to control the amount of photocatalyst for redox reactions (in Table 2).

The defects in GO enhance the interaction between ZnO NPs. Interfaces to ZnO and GO improve the photo electron mobility from ZnO to GO and reduce the recombination rates, increasing the photoactivity of the catalyst and reducing the catalyst amount for the reaction. The increase in polar facets reasonably increases the efficacy of the catalyst[111]. Pruna, A., et al., ZnO/GO hybrid synthesized by electrochemical deposition. The bandgap is reduced, and the effenciay is improved to 10 folds. The increased oxygen vacancies and high polar interfacial surfaces enhance photocatalytic activity. 99% of Methylene blue (MB) photo decay under UV irradiation in 120 minutes[112]. The graphene sheets trap electrons and reduce the charge recombination rate, which is responsible for the excellent performance relative to the other samples in the study. However, the dose of the pollutant is very low, which does not properly anticipate the performance for commercial use.

$C_3N_4$ is another carbon-based material extensively used for photocatalytic activity. A combination of both $C_3N_4$ and ZnO must exhibit efferent performance. Md Rosli, N.I., et al., coted the surface ZnO NPs with $gC_3N_4$ by impregnation. The surface modification enhances the degradation ability to 99% phenol degradation in 60 minutes under simulated sunlight irradiation (in Figure 8: (b)). The HR-TEM image clearly expresses the 4.2 nm coating of $gC_3N_4$ over ZnO (in Figure 8 (a)). The bandgap is decreased to 3.28 eV and the surface area to 2.56 m2/g-1. The particle size lies between 200 nm to 400 nm. The decrease in photoluminescent intensities indicates the effective synergic effects of the catalyst for photocatalytic activity[113]. Resulting in increased photo activity. $gC_3N_4$ increase in hybrid enhances the trapping of charges, prolongs the electron's lifespan, and reduces the recombination rate. The photocatalyst used for model study is huge, which does not make the ZnO/$gC_3N_4$ an effective option for commercial use (in Table 2).

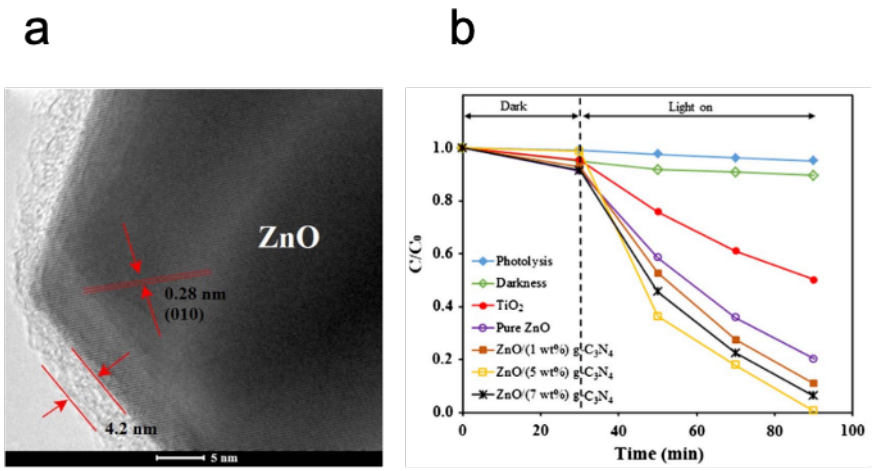


*Figure 8. (a) HRTEM images of ZnO (5 wt%) g-$C_3N_4$ photocatalyst (b) Phenol degradation using various photocatalysts.*[113] *Reprinted with permission from ref. 7*

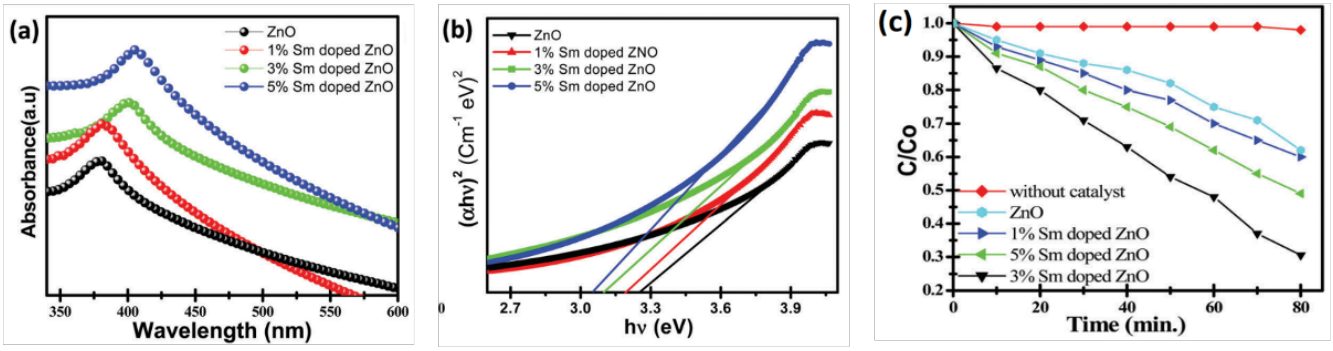


*Figure 9. (a) UV-visible spectra, (b) Tauc plot* ***(c)*** *Photocatalytic degradation of MG under the irradiation of visible light over the ZnO and Sm Sm- ZnO NPs*[114]*. Reprinted with permission from ref. 8*

Faraz, M., et al., used a gel combination route to dope ZnO with Sm. Photocatalytic activity in the visible range is for malachite green (MG) degradation. Band gap and crystallite size were reduced to 3.05 eV (in Figure 9 (a and b)) and 29.3 nm. In 80 minutes, MG decays up to 99% in the visible range (in Figure 9: (c))[114]. The total organic carbon decrease is directly proportional to MG degradation. The aggravated decomposition of dye is due to the rapid decay of aromatic intermediates. The separation of charges is due to the 4f orbital of Sm2+ ion. This result in the effective performance of Sm-ZnO photocatalyst. However, inorganic ions' presence is reported to cut down the photocatalytic activity, moreover the toxic effects of Sm metal are also not supported for the water treatments.

Besides being effective in the visible range, active, environment friendly and nontoxicity of catalyst is also a huge concern. As the residue catalyst in main drinkable water will be affecting the pollution. Araujo, F.P., et al., created a novel green photocatalyst. Karaya gum and Arabic gums are embedded in ZnO NPs by the sol-gel method. The activity is observed in the visible range for decomposition of methylene blue. Photo luminance (PL) emission is observed in the visible range of mesoporous structure with a pore size of 0.143 $cm^3/g$ for Arabic gum and 0.117 $cm^3/g$ for Karaya gum with a bandgap of 2.98 eV and 2.95 eV, respectively. The degradation efficiency was reported to be 91 % in karaya gum and 81.5% in Arabic gum under visible range in 120 minutes (in Figure 10 (a)). Multiple cycle study no significant change in photocatalytic activity (in Figure 10 (b))[115]. AGZ and KGZ are an attractive option for photocatalytic degradation. The effenciay ought to be increased along with detail study of multiple factors such as pH, temperature, light intensity, exposure time and etc before commercial use.

ZnO NPs active surface area and weak link to the surface atoms make them an attractive option for photocatalytic reaction. The availability of the charge on the surface facilitates the

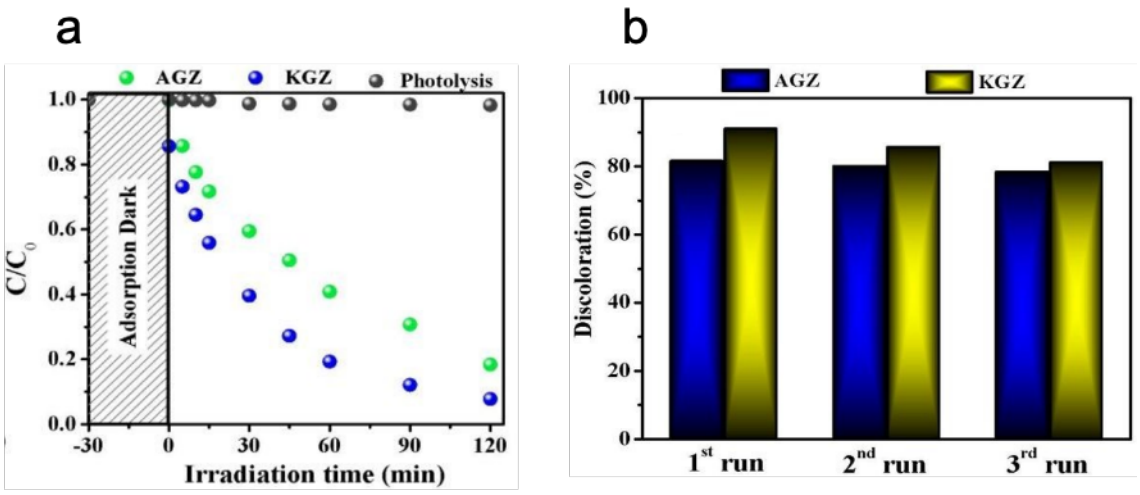


*Figure 10. (a) $C/C_0$ ratio as function of the irradiation time in photolysis of AGZ and KGZ; (b) Cyclic study for AGZ and KGZ nanoparticles in MB discoloration*[115]*. Reprinted with permission from ref. 9*

degradation of organic pollutants and aggravates the decomposition of intermediates. The increased charge separation and prolonged lifetime of charges are important factors for the increased efficiency of the catalyst. Summary of 0D nanostructures and their photocatalytic performance is shown in Table 2 and 3.

## One-dimensional ZnO

The interfaces between the catalyst and organic pollutants are responsible for photocatalytic reactions. The engineered morphology, modified nanostructures and activated surfaces majorly affect the performance of photocatalyst.[116] Low crystallinity and high defects in 1D nanostructures increase photocatalytic activity. The reduced recombination rate and longer lifetime of charges increase the effenciay of the photocatalyst. The excess number of hydroxyl groups bond with the catalyst and enhance the photoactivity[117].

### *Nanobelts*

Nanobelts are an emerging morphology exploited for photocatalytic purposes because of their single crystalline structure along the surface. Understanding electron transfer in 1 dimension, while a wider surface is exposed, is relevant to the other 1 D nanostructures.

Sun, T., et al., prepared ZnO nanobelts by carbothermal reduction route over SnO2-coated Si wafer as a substrate. ZnO nanobelts were photoactive in UV light to degrade methyl orange up to 94% in 5 hours. The width of the belts was in hundreds of nm with a length of micrometers. The absorption edge was at 380 nm with PL response at 382 nm wavelength[116,118]. Size reduction is responsible for the increase in the surface-to-volume ratio. The ability of charge transfer on the surface is much improved, and effective surface area is increased hence the performance. The ample time for photodegradation has urged the researchers to investigate further in this direction.

Likewise, another study is conducted by Wang, M., et al., to increase the photoactivity in ZnO nanobelts. The porous nanostructure was exploited with increased surface area. Oxidized ZnSe nanobelts prepared ZnO nanobelts with $H_2$-assisted thermal evaporation. The ZnO nanobelts have a slight decrease in efficiency after ten consecutive cycles of the degradation of methyl orange. The photodegradation reaction was performed in a mercury lamp with a wavelength of 365 nm. SEM and TEM results show high porosity; hence a large number of active sites were available for redox reaction (in Figure 11: (a-c))[119,120]. The cracks capture $O_2$* ions and reduce the recombination rate of charges. The performance is relatively improved from the previous study, but the designed photocatalyst is still unsuitable for extensive water treatment use. The excessively high dose of photocatalyst (in Table 3) and non-reproducibility are limiting factors.

Another approach to increase the effenciay is developed by Li, X., et al., Hydrothermal method synthesizes ZnSe/ZnO heterostructure. For the discoloration of RhB in the visible range. The activity is reported to be much more effective than the pure ZnSe and ZnO nanobelts. Moreover, the stability of the catalyst is effectively high[121]. The increase in performance is due to fast charge separation and a lower recombination rate. However, the ZnSe toxic nature cannot be ignored for water treatments.

$CeO_2$ is another well know heterogeneous photocatalyst[122,123]. A combined heterojunction of ZnO and $CeO_2$ is a logical approach to increase the effenciay[124–126]. Zhang, Qi., et al., syn-

*Table 2. The zero-dimensional ZnO nanostructures*

| Improvisation | Method | a (A°) | c (A°) | Crystalline size (nm) | Particle size (nm) | Surface area ($m^2g^{-1}$) | PL (nm) | $\lambda_{max}$ (nm) | Band gap (eV) | Ref |
|---|---|---|---|---|---|---|---|---|---|---|
| **QUANTUM DOTS** | | | | | | | | | | |
| ZnO QDs | Modified wet chemical | - | - | 2.9 | - | 312.10 | - | 315 | 3.57 | [92] |
| ZnO/RE (Eu, Er, Tb, Yb, Ho and La) metals | Sol-gel | 3.247 | 5.179 - 5.198 | - | - | - | 545 | 340 | - | [93] |
| ZnO QDs/CuO NSs | Hydrothermal | - | - | 3.2 | - | - | - | 350 | 1.86 | [98] |
| SZ/g-$C_3N_4$ | In-situ co-pyrolysis | 2.6 | - | - | - | 46.38 | 442 | 360 | 2.75 | [94] |
| ZnO/rGO | Simple chemical precipitation and hydrothermal | 2.3 | 1.56 -1.35 | 4.5-3.2 | - | 135 | - | 590 | 2.1 | [99] |
| ZnO/Ag | Facile sol gel | 2.6 | 2.4 | 10.71, 12.87 | - | | 530 | 435 | 2.92 | [100] |
| ZnO QDs/CuO NSs | Hydrothermal | | | 3.2 | | | | 360 | 1.86 | [101] |
| ZnO QDs/ $TiO_2$ | Sol-gel assisted hydrothermal | | | 9.22 | | | 559 | | 3.24 | [103] |
| ZnO QDs@$ZrO_2$-$TiO_2$ | Sol–gel reaction and colloidal template | 3.8 | 9.6 | 15.78 | | 46.14 | 470 | 325 | 2.95 | [102] |
| **NANOPARTICLES** | | | | | | | | | | |
| ZnO NPs | Sol–gel | | | | 15-24 | | | 460 | - | [104] |
| ZnO/$SnO_2$ | Sol–gel | 3.22 | 5.2 | | | | | | 3.25 | [105] |
| Al-ZnO | Sol–gel | | | 10 | | | | 370 | 2.93 | [107] |
| Al-ZnO | Sol–gel combination | 2.6 | | 6.4 | 7 | | | 400 | 3.23 | [108] |
| L-CQDs/ZnO | Steaming ammonia and hydrothermal | | | | 10-40 | | 475 | | 2.69 | [110] |
| ZnO/GO | Electrochemical deposition | | | | | | | | - | [112] |
| ZnO/g$C_3N_4$ | Impregnation | 2.8 | | | 200-400 | 2.56 | 487 | | 3.28 | [113] |
| Sm-ZnO | Gel combination route | 3.27 | 5.25 | 29.3 | | | | 400 | 3.05 | [114] |
| AGZ | Sol–gel | 3.25 | 5.21 | 22 | | 32.59 | 440, 473 | 416 | 2.95 | [115] |
| KGZ | | 3.25 | 5.2 | 21 | | 27.59 | | 420 | 2.98 | |
| | | | | | | | 478, 549 | | | |

*Table 3. The zero-dimensional ZnO nanostructures and their perfromance*

| Improvisation | Performance Active range | Pollutant | % decay | Decay time (min) | Pollutant Dose (mg/l) | Catalyst dose (mg/l) | Reaction temp (°C) | Cycles | Ref |
|---|---|---|---|---|---|---|---|---|---|
| | | | **QUANTUM DOTS** | | | | | | |
| ZnO QDs | Sun light | CBBR | 25% | 330 | 2.8 | 50 | RT | 9 | [92] |
| ZnO/RE (Eu, Er, Tb, Yb, Ho and La) metals | UV-Vis | Phenol | 90% | 60 | 20 | 50 | 10 | - | [93] |
| ZnO QDs/CuO NSs | Sunlight and UV | TeNT | 75% | 90 | 1 | 10 | 25 | - | [98] |
| SZ/g-$C_3N_4$ | Visible | RhB | 99% | 60 | - | 40 | RT | 4 | [94] |
| ZnO/rGO | Visible | TC<br>Cr (VI) | 68%<br>84% | 120 | 20 | 50 | RT | - | [99] |
| ZnO/Ag | Sunlight | MB | 99% | 80 | 1 | 20,000 | RT | 3 | [100] |
| ZnO QDs/CuO NSs | UV | MPTP<br>TeNT | 80% | 60 | 1 | 100 | 250 | 10 | [101] |
| ZnO QDs/ $TiO_2$ | Fluoresce light | TC | 98% | 90 | 20 | 250 | RT | 4 | [103] |
| ZnO QDs@$ZrO_2$-$TiO_2$ | UV, Visible and Simulated sunlight | CR | 94% | 120 | | | RT | 3 | [102] |
| | | | **NANOPARTICLES** | | | | | | |
| ZnO NPs | Visible | MO | 99% | 180 | 20 | 40 | RT | - | [104] |
| ZnO/$SnO_2$ | UV | MO | 99% | 35 | 10 | 60 | RT | - | [105] |
| Al-ZnO | UV | MO | 65% | 180 | 15 | 30 | RT | - | [107] |
| Al-ZnO | UV | MO | 99% | 30 | 200 | 700 | RT | - | [108] |
| L-CQDs/ZnO | Visible | Phenol | 99% | 300 | 50 | 1000 | RT | 10 | [110] |
| ZnO/GO | UV | MB | 99% | 120 | 3 | | RT | | [112] |
| ZnO/g$C_3N_4$ | Simulated sunlight | Phenol | 99% | 60 | 5 | 1000 | RT | - | [113] |
| Sm-ZnO | Visible | MG | 99% | 80 | 5 | 100 | RT | - | [114] |
| AGZ<br>KGZ | Visible | MB | 81.5%<br>91% | 120 | 4 | 500 | 25 | 3 | [115] |

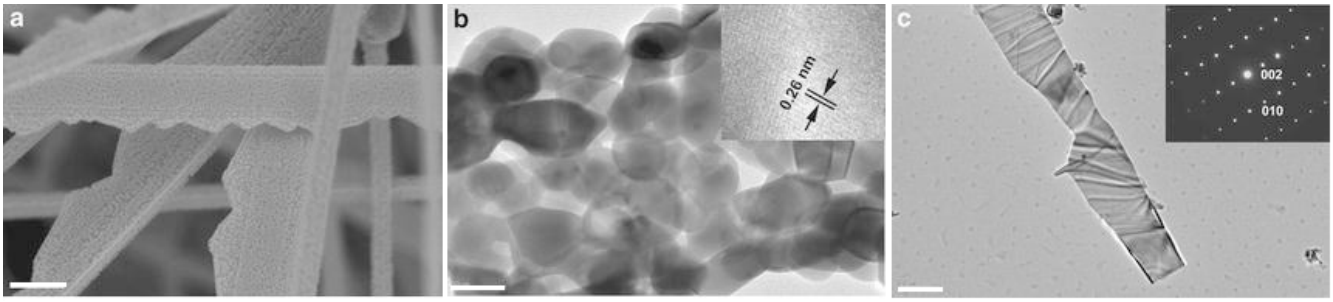


*Figure 11. (a) SEM image of the porous ZnO nanobelts on Si substrate. The scale bar is 500 nm. (b) TEM image of a single porous ZnO nanobelt. The inset is HRTEM of several ZnO nanoparticles. The scale bar is 50 nm. (c) TEM image of a single solid ZnO nanobelt. The inset is SAED. The scale bar is 500 nm*[119]*. Reprinted with permission from ref. 19*

thesized hybrid $CeO_2$/ZnO nanobelts by one-step electrospinning method. The methylene blue (MB) is used as a model dye to degrade. In 60 minutes, the degradation is almost 95% under visible light. The nanobelts' diameter range between 340-410 nm (in Figure 12: (a-c)) with a bandgap of 2.91 eV. The surface area increases to 165.52 $m^2/g$ with a decrease in average pore size of 3.2 nm. The decrease in total organic carbon after the degradation of MB indicates high efficiency. Despite that, the performance is decreased after four cycles[127]. The increase in photoactivity is 3-fold due to the prolonged separation of electron/hole pair compared to the pristine CeO2 nanobelts. The increase in surface area is responsible for the TOC decrease and increase in the overall performance of the photocatalyst. The lack of reusability directly influences the commercial usage.

ZnO nanobelts are widely explored nanostructure as photocatalysts. The single crystal facet at the surface enables profound electron mobility and better photoactivity. The decrease in crystalline size and increase in the surface area enables a larger number of organic pollutants to degrade at the surface. The heterojunction and porous nanobelts structure increase the electron capturing and superoxide ions and reduce charge recombination.

### *Nanorods*

The nanorods are another one-dimension nanostructure exploited for photocatalytic studies. The high aspect ratio and the surface-to-volume ratio dictate the catalyst's performance. Many techniques are implied to develop an effective photocatalyst by ZnO nanorods.

Fu, D., et al., reported ZnO nanorod for photoactive degradation of MB up to 80% in 40 min. Nanorods were synthesized by the combination of facile sol-gel and hydrothermal methods. Bandgap decreased to 3.17 eV with an average length of 51 nm and an average diameter of 12 nm. The performance is slightly decreased after five cycles[116,128]. The humongous amount of catalyst is not encouraging for commercial use (in Table 3). The efficiency was reported to be more effective than P25 ($TiO_2$) commercially used photocatalyst, which urges further research for water treatments.

Another effort was made to degrade MB by ZnO nanorods of different aspect ratios and variations in annealing temperatures by Zhang, X., et al., Mechanical assisted thermal decomposition method in an aqueous solution was used to synthesize ZnO nanorods. The aspect ratio is directly proportional to the photocatalytic activity and oxygen defects increase. The methylene blue was degraded up to 99% in 80 mins under high-pressure sodium lamp with wavelength of 400–650 nm. The band gap decreases to 3.27 eV. Extensively long nanorods of 800 nm with diameter range between 30 to 50 nm. At higher annealing temperatures and shorter lengths, nanorods were formed (in Figure 13). Photocatalytic effenciay also decreases due to the reduction in surface area and aspect ratio[117,129]. During annealing, the crystalline phase and facets on surfaces remain the same. However, the aspect and defects ratios vary, which are responsible for the different performance effects. The charge separation is due to the variation in aspect ratio and facets of electronic structures. The surface defects enhance electron trapping, and reduction in recombination increase photoactivity. The effenciay is almost same after 5 cycles but the high dose (in Table 3) and lack of reproducibility reduce the scope of the photocatalyst.

Hsu, M. H., et al., decoration of Ag-doped ZnO nanorods over stainless steel mesh shows sensitivity to visible light. MO and food black 2 (FB2) dyes were targeted during the study (in Figure 14: (b)). The bandgap was reduced to 3.1 eV with 0.26 nm d spacing (in Figure 14: (a)). The range of diameter lies 60 to 110 nm. The enhanced hydrophilic nature and heterogeneous interface of Ag-ZnO increase its effenciay. The effenciay was reported to be almost 99% for both dyes after three successive cycles[130,131]. The stainless-steel wire mesh is supportive of the flow of photo degraded electrons. The enhanced life span of electrons decreases the recombination of charges which is mainly responsible for enhanced photocatalytic activity. The charge separation reduces the issue of photo corrosion as well. Despite the performance, the possibility of mesh oxidation and polluting the drinkable water cannot be ignored. However, the above mentioned photocatalyst can be used for water reclamation other than drinking water.

Sin, J. C., et al., synthesized Sm doped ZnO nanorods effenciay is observed to have higher performance relative to the pristine ZnO nanorods. The red shift in the band gap is 3.23 eV with the photoactive range in visible light. The diameter decreases with Sm doping to 43-103nm from 68-139 nm, and the length was hundreds of nm. Absorbance edge has also shown a reduction from 400 nm to 390 nm. Photodegradation of phenolic compounds during multiple cycles up to 99%[132]. The effenciay of Sm/ZNRs is enhanced due to the increase in reactive sites. The surface area and presence of catalyst sites are reasonably larger than the pristine ZnO nanorods. The performance for phenolic compounds is better than pure ZnO nanorods, i.e., 71.2% and commercial TiO2, i.e., 58.9%. However, the high toxicity of Sm is the major limiting factor of water purification application.

ZnO-based visible light active photocatalyst constraints are not limited by doping, but the heterojunction and hybrids are also effective and advanced approaches. Kumar, S., et al., developed heterojunction of ZnO nanorods and graphene QDs by facile hydrothermal method. The bandgap of ZnO-GQDs was reduced to 3.08 eV with exceptionally long nanorods. Hetero-

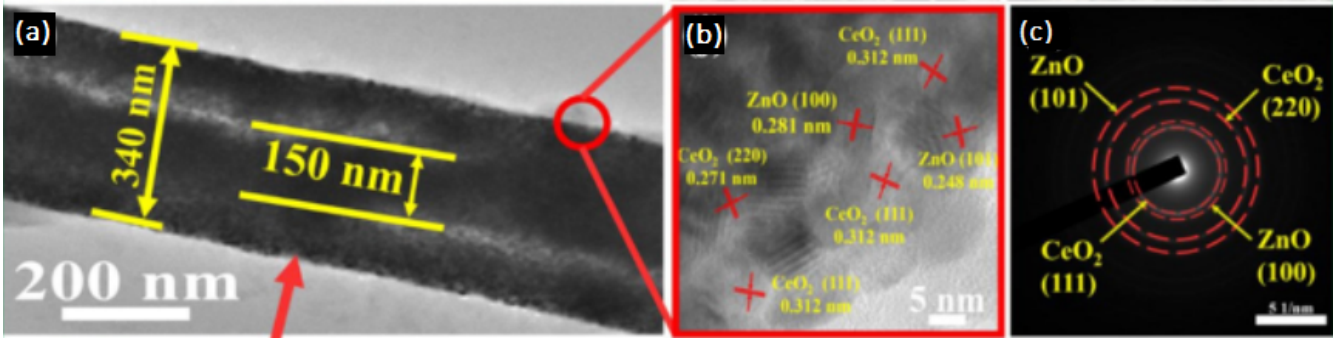


*Figure 12. **(**a) TEM; (b) HRTEM; and (c) the corresponding SAED images of $CeO_2$/Zn-0.03*[127]*. Reprinted with permission from ref. 20*

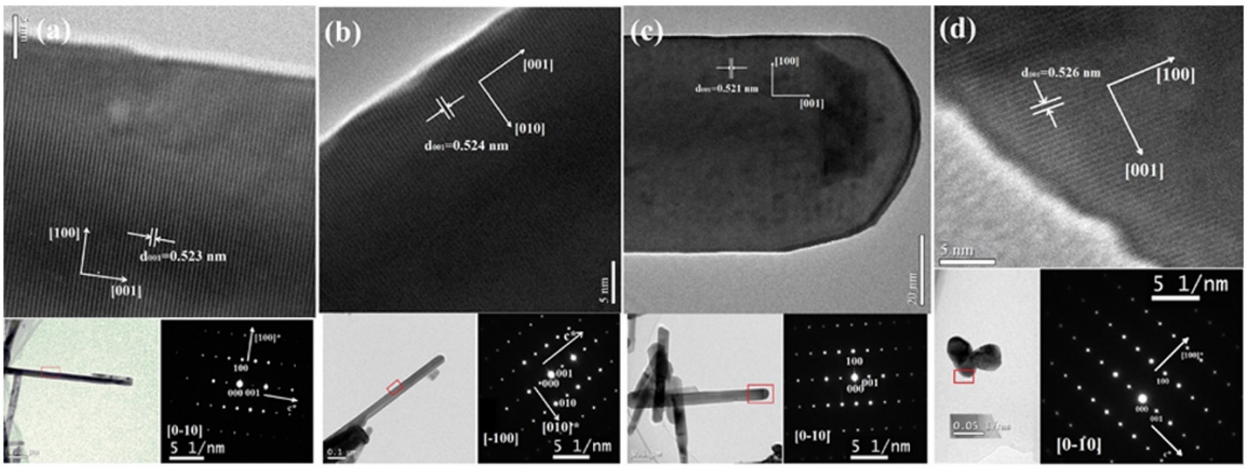


*Figure 13. **Figure 13:** HRTEM of as-synthesized ZnO under temperature of (a) 350°C, (b) 400°C, (c) 450°C, (d) 500°C.*[117] *Reprinted with permission from ref. 21*

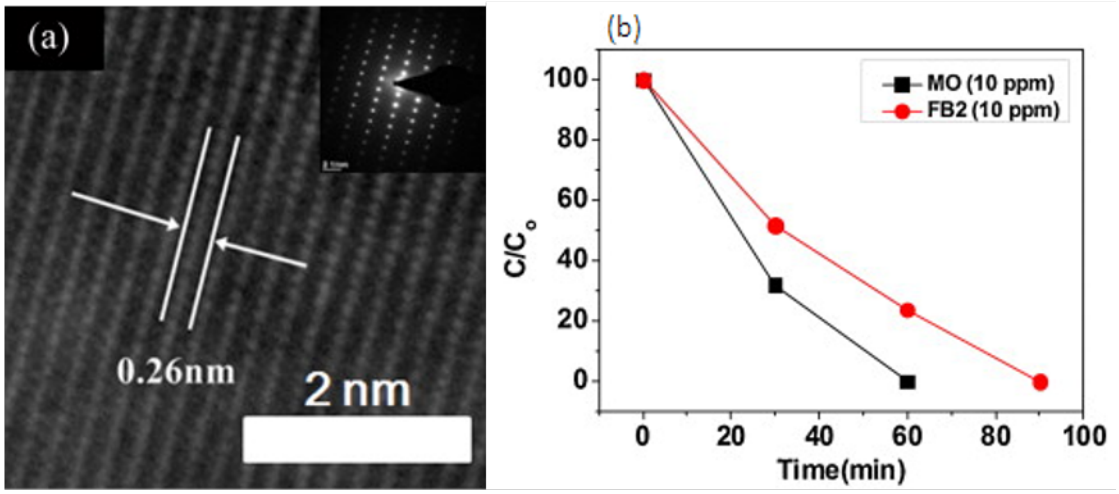


*Figure 14. (a) TEM; (inset**)** HRTEM images and SAED patterns of Ag-ZnO nanorods and (b) decolorization of MO and FB2 dye solutions (10 ppm), decolorization of MO dye solution*[130]*. Reprinted with permission from ref. 22*

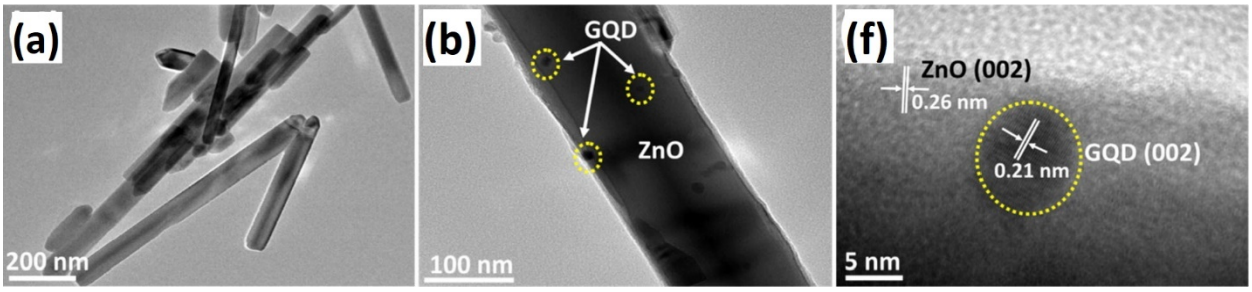


*Figure 15. TEM images of (a) ZnO nanorods, (b) ZGQD2 and (c) HRTEM image of ZGQD2*[133]*. Reprinted with permission from ref. 23*

junction shows photocatalytic activity in both UV and visible light. The MB and carbendazim fungicide (CZ) are reported to decay under sunlight up to 95% in 70 minutes. The TEM image of catalyst clearly exhibits 0.26 nm d spacing of ZnO (002) plane (in Figure 15). The surface area of 353.447 $m^2g^{-1}$ was reported with good adsorption capacity with organic pollutants, subsequently increasing the photocatalyst's efficiency. Moreover, the ZnO-GQD heterojunction can be recycled for degradation after recovering by centrifuging and thorough washing. The photocatalytic activity is 91% even after the four cycles, while the crystal structure is still intact [133]. The enhanced photoactivity is the attribute of better absorption of organic pollutants and photosensitization within the heterojunction, which enables the catalyst to absorb a wider range of sunlight. The effective charge carrier separation onto the surface of photocatalytic interfaces and faster rate of electron transfer was due to the better interaction at the interfaces between ZnO nanorods and graphene QDs. Despite the advantages the dose of the catalyst for photo reaction is huge which limits the usage at market level.

Xu, T., et al., developed a novel ternary photocatalytic system. ZnO nanorods hybrid with reduced graphene oxide (rGO) infused with $CuInS_2$ QDs were active in visible light. The ZnO nanorods are synthesized by the solid-state synthesis method, and the facile hydrothermal reaction is used to make a hybrid with rGO. $CuInS_2$ QDs were prepared with a one-pot colloidal chemistry method and later added with ZnO/rGO hybrid. Possible mechanism of exitron transportation during the reaction is shown in Figure 16. The hybrid maintained the length of ZnO nanorods at 50 to 100 nm, which assures the mechanical strength of ZnO nanorods. ZnO-RGO-$CuInS_2$ was responsive to RhB photoactive decay up to 99% in 120 min under visible light. [134]. The increase in performance is due to enhanced light absorption and charge transfer. Moreover, the synergic effect supports the degradation of organic pollutants. The system's lack of recombination and prolonged life of photoelectrons is a major attribute. The system needs further investigation for different factors such as the system's responsibility, the effect of intensity, pH, temperatures, and reusability before commercialization.

The crystalline phase, aspect ratio, facets and defects on the outer surface can be increased by doping, heterojunction, and hybrid formation. The same phase on the surface is a supportive point for the charge transfer along the surface. Whereas a charge separation and reduced recombination rate profoundly increase the performance. The effective surface area is another factor in utilizing the nanorod structures. However, the performance remains less than the zero-dimensional nanostructures due to their lack of surface area.

*Nanowires*

The easy synthesis of nanowires is one of the many reasons that scientists were more interested in their photocatalytic activity. The better control over this nanostructure enables researchers to exploit them for different applications.

Well-arranged ZnO nanowires were exploited for the degradation of MR in UV light by Liu, Y., et al., The c-axis growth of nanowires with 0.52 nm d-spacing. An average diameter was 120 nm on average, and the length of the nanowire was outstandingly long (3000 nm). The results of nanowire arrays were improved compared to nanorods arrays, 38% from 14.6%, respectively, along with the redshift in PL intensity to the visible edge. The enhanced oxygen deficiency was reported, which is a prime factor in the improved photodegradation performance [135,136]. The surface reaction of organic pollutants is a stepwise process of dispersion, diffusion, adsorption of organic dye and eventually desorption. Every step controls the performance of the photocatalysts, but dispersion is governing step. Effective surface area and oxygen defects promote photocatalytic activity. The efficiency of pure ZnO nanowires is not attractive for extensive use. However, the performance can be improved by deploying different strategies.

Doping is a well-known method for band tailoring and lowering the sensitivity to the longer wavelengths, which results in improved photocatalytic performance. Udom, I., et al., synthesized

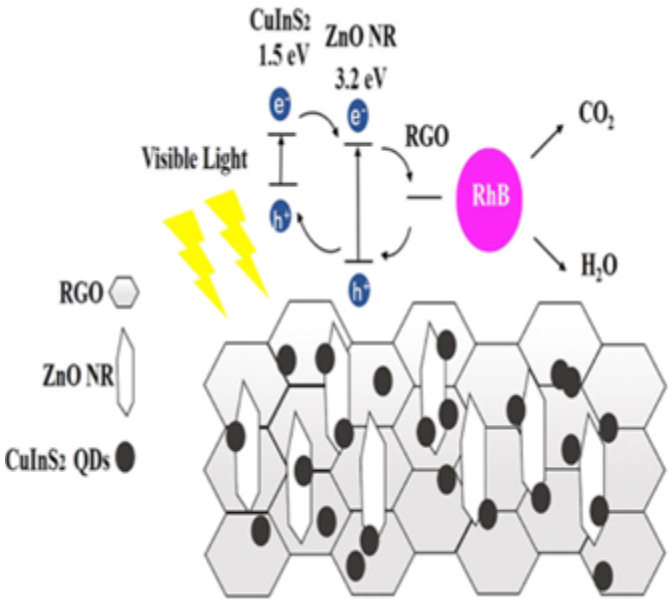


*Figure 16. Schematics of the ZnO-RGO-$CuInS_2$ [134]. Reprinted with permission from ref. 24*

Ag-doped ZnO nanowires have shown that the photodegradation of methylene orange in visible light in four hours is almost 1.2% better than in pristine ZnO nanowires. The Ag-ZnO were prepared by the scalable hydrothermal process with a diameter ranging between 40-70 nm and a length of a few hundred nm. The performance of Ag-ZnO has shown a decrease in four consecutive cycles [137]. The enhanced performance relative to pure ZnO nanowires is due to the electrons captured within the Ag-ZnO nanostructure. The reduced recombination rate is also a factor in influencing photoactivity. However, the performance is far less than other one-dimensional nanostructures.

The carbonaceous material has shown better performance for photodegradation. Ebrahimi, M., et al., decorated ZnO nanowires with graphene QDs are reported to improve the photocatalytic degradation of MB 3-fold in comparison to pristine ZnO nanowires. The nanowire was synthesized by anodizing Zn foil, and graphene QDs were obtained by the one-step electrochemical process led by spin coating for GQD/ZnO NWs hybrid formation. The absorbance edge was observed in the visible range. With a bandgap of 2.65 eV, the length of ZnO NWs was 1200 nm, and the diameter ranges between 170 to 250 nm [138]. Graphene QDs are an effective optical absorber in the visible range. The effective charge separation and increased surface area are responsible for the increase in performance. The performance is far less than the ZnO nanorods because of the lack of surface area and active reaction sites.

The ZnO nanowires are having large surface area and better-controlled growth. The electron capturing capacity is high, but the photocatalytic efficacy is far less than other zero-dimensional nanostructures. The aspect and surface-to-volume ratios are not as high as zero-dimensional nanostructures, and so do their performance.

### *Nanotubes*

Various ZnO nanostructures have been well studied in the context of their application in a photocatalyst. ZnO nanotubes are explored for photodegradation.

In-situ electrochemical etching of electrodeposited ZnO nanotubes was used to create ZnO nanotubes for degradation of MO as a probe pollutant by Xu, F., et al. Large surface to volume ratio of nanotubes an attribute to high photocatalytic activity. The length of nanotubes ranges between 300-400 nm with a bang bandgap of 2.4 eV due to the excessive surface defects introduced by etching. The effective surface area enables numerous organic pollutants to attach to the catalyst's surface. Moreover, the oxygen vacancies are easily excess to start a redox reaction. Quantum efficiency is improved by 23% compared to 3.53% in nanorods [139]. The ZnO nanotubes have better performance than other one-dimensional nanostructures. It has a better quantum efficiency of photo-generated electrons and a larger surface-to-volume ratio. The reusability and catalyst dose are factors yet to be investigated. The mechanical strength of the nanotubes is compromised due to excessive etching.

Chu, D., et al., synthesized ZnO nanotubes by facial two-step chemical bath method to decompose MO dye under UV light. The average length of nanotubes was ~600 nm. After five cycles, the effenciay was gradually decreasing [140]. Higher surface area,

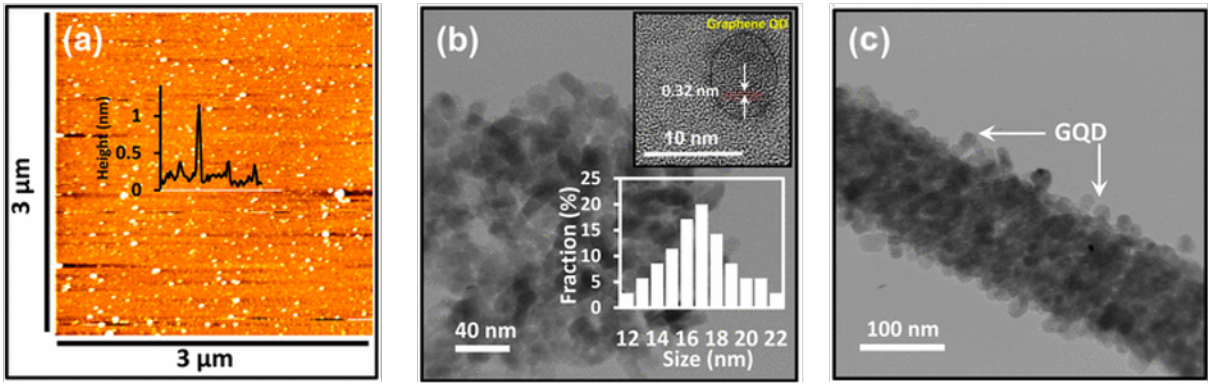


*Figure 17. (a) AFM image of the GQDs. The inset shows the height profile of GQDs corresponding to the white line. (b) TEM image of the GQDs. (Top inset) HRTEM image and (Bottom inset) size distribution. (c) TEM images of GQD (0.4 wt %)/ZnO NWs. [138] Reprinted with permission from ref. 138*

polar facets and oxygen vacancies are major attributes of enhanced photo activity. The decrease in performance after cyclic use, the dose of catalyst is unclear, reproducibility and high pH requirement are quite discouraging for excess use.

H. Wa et al., synthesized porous ZnO nanotube. Enhanced photocatalytic activity for degrade MO was observed due to the enhanced surface area by the nonuniform distribution of the nanohole over the surface. In Figure 18, the mechanism of synthesis of porous ZnO nanotubes has been shown. The activity was observed in the UV range. Figure 18 (f) has shown the mechanism of the accelerated diffusion of dye molecules into the inner part of the nanotube to enhance photocatalytic activity. The ZnO nanotubes of a uniform length of 500 nm and diameter of 250 nm were formed.[116,141]. The porous nanotubes have a large surface area. Both inside and outside surface areas contribute to photocatalytic activity. The fast diffusions enabled by nanoholes enhance the chances of encountering the photogenerated electrons with organic dye. Hence increasing the photocatalytic activity. After multiple cycles, the performance reduced considerably due to the low mechanical strength.

The nanotubes are the one-dimensional nanostructure which shows higher photocatalytic activity. Because of the larger surface area, both inside and outer surfaces are exposed for the reaction. The oxygen vacancies and defects further hence the activity. Higher quantum effenciay is reported by ZnO nanotubes. Summary of 1D nanostructures and their photocatalytic performance is shown in Table 4 and 5.

## Two-dimensional ZnO

### *Nanosheets*

ZnO nanosheets are highly affected by the specific direction and polar faces. A large surface area provides numerous reactive sites for degradation. In the above discussion, zero and one dimensions of ZnO nanostructures have shown higher efficiency for photocatalytic activity. The two-dimensional structure must also be studied for water purification applications.

Wang, M., et al., synthesized ZnO nanosheet by employing complexing agent $NH_4$ to turn the $Zn^{2+}$ and $OH^-$ ions ratio by solvothermal routes. The lattice constant "a" was 1.4 A°, and "c" was 2.8 A°, with a thickness of 18 nm. The effect of ZnO crystal on photodegradation is studied. 90% of MB is achieved in four hours due to the reactive face of ZnO $(10\bar{1}0)$ at the surface. The performance decrease during three cycles[142,143]. The photocatalytic activity is directly dependent on the facet. The increase in ZnO $(10\bar{1}0)$ of ZnO nanosheets increases the photo activity performance. The size of the ZnO nanosheet is less important than the morphological arrangement of the reactive site on the surface. The reported decay time was very long

Liu, D., et al. make another effort; the solvothermal annealing method uses ZnO porous nanosheets with a thickness of 10-30 nm. An enhanced surface area of 39.18 $m^2g^{-1}$ is reported in ZnO nanosheets. Phenol is used as an organic probe pollutant under UV radiation. The photodegradation is reported to be better than commercial ZnO photocatalyst[144,145]. Defects in surface and bulk material play a major role in photocatalytic performance. The decrease in the relative concentration of defects from bulk to surface significantly enhances the charge separation. The defects on the surface trap electrons and act as adsorption sites of organic pollutants for degradation. Prolonged charge separation and better adsorption increase photocatalytic activity. Bulk defects only serve as charge traps and increase the separation, but fewer adsorption sites are provided. The larger surface area of porous ZnO nanosheets provides numerous active sites for photocatalytic reaction, better diffusion, and mass transportation of organic dyes. Efficient flow

*Table 4. The One-dimensional ZnO nanostructures*

| Improvisation | Method | a (A°) | c (A°) | Length (nm) | Width (nm) | Surface area ($m^2g^{-1}$) | PL (nm) | Absorbance Peak (nm) | Band gap (eV) | Ref |
|---|---|---|---|---|---|---|---|---|---|---|
| **NANOBELTS** | | | | | | | | | | |
| ZnO | Carbothermal reduction route | 2.6 | - | - | 100-500 | - | 382 | 380 | - | [118] |
| ZnO | Thermal evaporation | 2.6 | - | - | 50 | - | - | - | - | [119] |
| ZnSe/ZnO | Hydrothermal | - | - | - | - | - | - | - | - | [121] |
| $CeO_2$/ZnO | Electro spinning | 2.8 | 2.4 | - | 340-410 | 165.52 | - | - | 2.91 | [127] |
| **NANORODS** | | | | | | | | | | |
| ZnO | Sol-gel and hydrothermal | - | - | 51 | 12 | - | 468 | - | 3.17 | [128] |
| ZnO | Thermal decomposition | | 5.23 | 800 | 30-50 | 8.02 | 510 | 373 | 3.27 | [117] |
| Ag-ZnO | Seed method | 2.6 | - | - | 60-110 | - | - | - | 3.1 | [130] |
| Sm/ZNRs | Solvothermal | 2.6 | - | 100-300 | 43-103 | - | 425 | 390 | 3.23 | [132] |
| ZnO-GQD | Hydrothermal | 2.6 | - | 1000 | - | 353.447 | 440, 490, 510 | 402 | 3.08 | [133] |
| ZnO-RGO-$CuInS_2$ | Solid-state synthesis and hydrothermal | - | - | 50-100 | - | - | - | 380 | - | [134] |
| **NANOWIRES** | | | | | | | | | | |
| ZnO | Solution-phase | - | 5.2 | 3000 | 120 | - | 380 | 480 | - | [136] |
| Ag-ZnO | Scalable hydrothermal process | - | - | 300-500 | 40-70 | - | - | 400 | - | [137] |
| GQD/ZnO NWs | Electrochemical, anodization process and spin coating method | - | - | 1200 | 170-250 | | 450 | | 2.65 | [138] |
| **NANOTUBES** | | | | | | | | | | |
| ZnO | In-situ electrochemical etching of electrodeposited | - | - | - | 300-400 | - | 376 530 | - | 2.4 | [139] |
| ZnO | Facial two-step chemical bath | - | - | ~650 | - | - | 381 | - | - | [140] |
| ZnO | Facile hydrothermal | 2.6 | - | 500 | 250 | | | | | [141] |

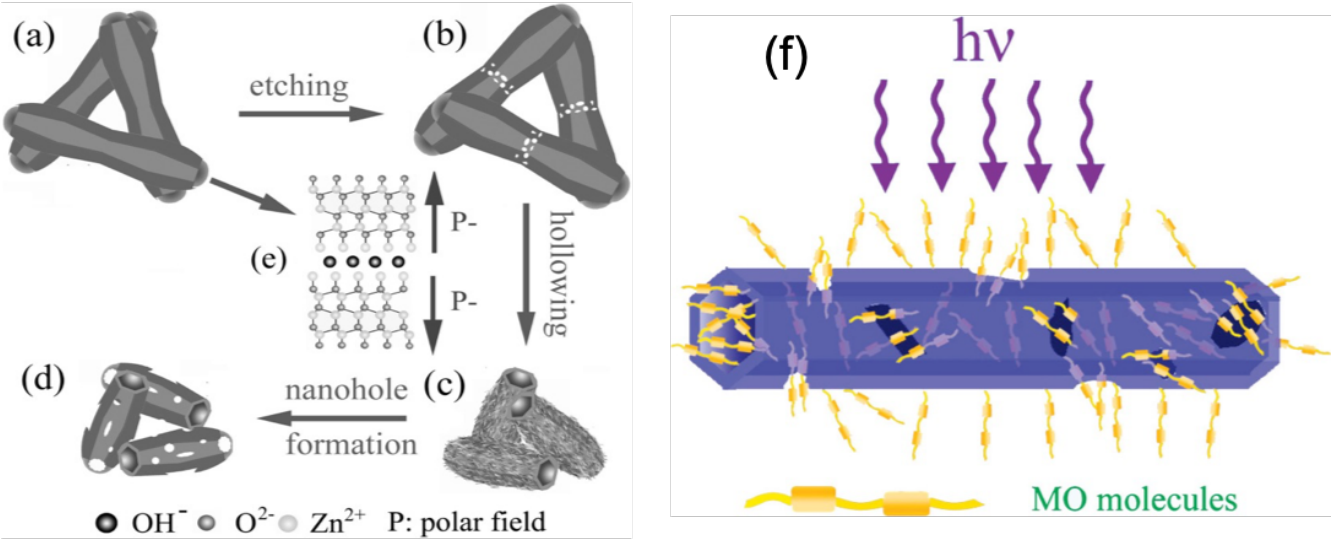


*Figure 18. Schematic illustrations of the formation mechanism of the porous ZnO nanotubes: (a) formation of a paired nanorod, (b) etching at the center of the paired nanorods, (c) further etching leading to the splitting and hollowing of the paired nanorods, and (d) radial etching leads to the formation of nanoholes on the side walls. (e) polar field counterbalance leads to the formation of the paired nanorod. (f) Schematic illustration of the accelerated diffusion of dye molecules into the inner part of the nanotube leading to high photocatalytic activity[141]. Reprinted with permission from ref. 26*

of hydroxyl radical along the surface improves the photocatalytic activity. A high dose of the photocatalyst was used in the photodegradation reaction.

To enhance the photoactivity of ZnO nanosheets, Harish, S., et al., decorated them with SnO NPs. The system is synthesized by hydrothermal method using ethylenediamine (EDA) as a capping ligand. MB is the targeted dye, and the degradation is reported to be much higher. With the optimized addition of SnO, the performance is 90% decay in 6 minutes. The effenciay decreased to 89% after 3 cycles. The further addition of SnO decreases the photocatalytic efficacy. The chances of agglomeration and oxidation of SnO increase with the increase in percentage addition[146]. The successful coupling with ZnO/SnO enhances photo activity due to the heterojunction, better charge separation and increased surface area. The effenciay of ZnO is reported to be highest in heterojunction, but the oxidizing of SnO limits the commercial use of the ZnO/SnO photocatalytic.

The ZnO nanosheets show higher photocatalytic performance due to the large surface area and specific crystal plain on the surface, which enables rapid charge flow and provides more reactive sites for redox reactions. The performance in ZnO nanosheets mainly depends on the reactive facets and defects on the surface. Higher the defects, the higher the performance. The enhanced separation of charge and increased oxygen vacancies are the outcomes of surface defects. The heterojunction and decoration of ZnO nanosheets are good options for achieving an effective photocatalytic. Summary of 2D nanostructures and their photocatalytic performance is shown in Table 6 and 7.

## Three-dimensional ZnO

### *Nanoflowers*

The large surface-to-volume ratio and better light scattering capability make nanoflower an efficient nanostructure for photocatalytic activity as it can harvest multiple excitons from incident light by successive scattering of incident radiation. Numerous efforts are reported to synthesize ZnO nanoflowers for photocatalytic application.

One such effort is made to synthesize ZnO nanoflowers via a simple low temperature hydrothermal assisted route in the absence of surfactants by Y. Wang, X. Li, et al., s. the reported d-spacing TEM images were 0.26 nm (in Figure 19) with a diameter of nanoflowers in few thousand nm and thickness of 80-150 nm. The decomposition of 4-chlorophenol (4-CP) organic dye was done under UV radiation up to 80 % in 120 minutes, relatively faster than ZnO nanorods. The better performance is due to the charge-capturing ability of oxygen vacancies[147,148]. Higher oxygen vacancy in ZnO nanoflowers acts as the reactive centre. The large surface area and complex morphology cause multiple scattering of light; hence the photocatalytic activity is enhanced. THE ZnO nanoflowers are composed of multiple nanorods grown from a single nucleation point. The replication of such a structure is a huge challenge.

Recently an effort has been made to develop well-aligned ZnO nanoflowers to degrade MB by microwave-assisted growth under solar light by

*Table 5. The one-dimensional ZnO nanostructures and their performance*

| Improvisation | Active wave-length range | Pollutant | % decay | Decay time (min) | Pollutant Dose (mg/liter) | Catalyst dose (mg/liter) | Reaction temper-ature (°C) | Cycles | Ref |
|---|---|---|---|---|---|---|---|---|---|
| **NANOBELTS** | | | | | | | | | |
| ZnO | UV | MO | 94% | 300 | 15 | - | 25 | - | [118] |
| ZnO | Mercury lamp | MO | 99% | 160 | 4 | 1600 | RT | 10 | [119] |
| ZnSe/ZnO | Visible | RhB | - | - | - | - | - | - | [121] |
| CeO2/ZnO | UV-Visible | MB | 95% | 60 | 15 | 20 | RT | 4 | [127] |
| **NANORODS** | | | | | | | | | |
| ZnO | Xe lamp | MB | 80% | 40 | 20 | 600 | 25 | 6 | [128] |
| ZnO | High-pressure sodium lamp | MB | 99% | 80 | 5 | 500 | 35 | 5 | [117] |
| Ag-ZnO | Visible | MO<br>FB | 99%<br>99% | 60<br>90 | 10 | - | 25 | 3 | [130] |
| Sm/ZNRs | Visible | phenol | 99% | 480 | 20 | 1000 | RT | 3 | [132] |
| ZnO-GQD | UV- Vis-ible | MB<br>CZ | 95% | 70 | 3<br>1 | 400 | RT | 4 | [133] |
| ZnO-RGO-CuInS2 | Visible | RhB | 99% | 120 | 5.6 | 250 | RT | - | [134] |
| **NANOWIRES** | | | | | | | | | |
| ZnO | UV | MR | 38% | 300 | 67.3 | - | RT | - | [136] |
| Ag-ZnO | Visible | MO | 99% | 240 | 2 | - | 19.8 | 4 | [137] |
| GQD/ZnO NWs | Visible | MB | 78% | 180 | 15 | 300 | RT | - | [138] |
| **NANOTUBES** | | | | | | | | | |
| ZnO | UV | MO | 100% | 95 | - | - | RT | - | [139] |
| ZnO | UV | MB | 97% | 80 | 20 | - | RT | 5 | [140] |
| ZnO | UV | MO) | 100% | 60 | 16 | 187 | RT | 5 | [141] |

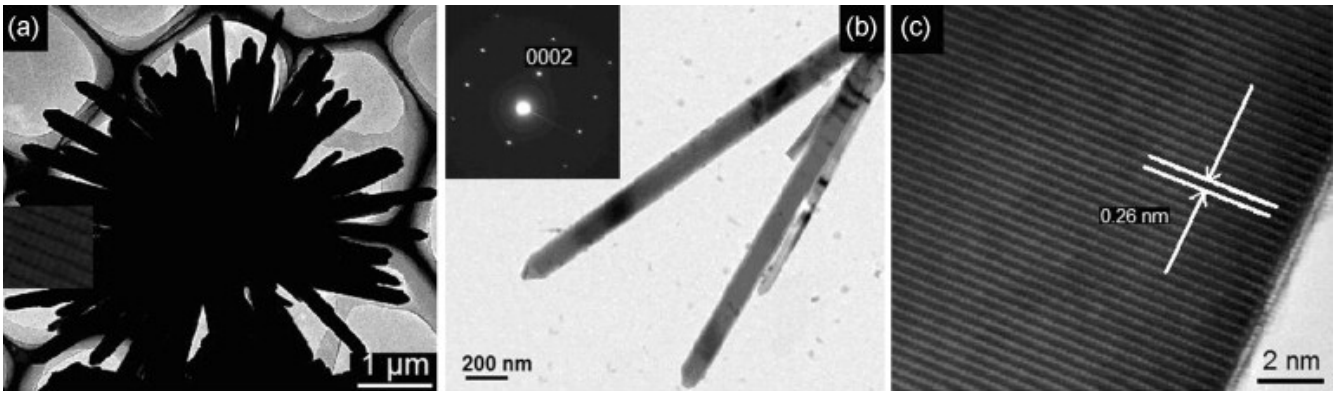


*Figure 19. TEM images of the ZnO nanoflowers (a) at Low magnification, (b) at higher magnification (SAED patterns.) and (c) HRTEM image[148]. Reprinted with permission from ref. 38*

A. Das, et al. the average thickness of nanoflowers was 35.04 and diameter of 91 nm. The surface area increased to 29.3 $m^2g^{-1}$ with a bandgap of 3.2 eV[149]. The reduced charge recombination, efficient photon absorption, more effective surface area and multiple scattering within the petals of flowers enhance the photocatalytic performance. The microwave-assisted nanoflower shows higher photonic efficiency due to the optimal flower-like morphology. The spacing between the petals is ideal for solar light multiple scattering.

To enhance the performance ZnO nanoflowers surface was functionalized by nitrogen/ sulfur-doped carbon were synthesized by QDs by Qu, Y., et al., One-pot hydrothermal method is used to create the system. In Figure 20 schematic of the synthesis and photocatalytic mechanism of ZnO/N, S-CQDs nanoflowers in shown the hybrid was active in visible and near-infrared light. The average diameter of nanoflowers was in few hundred microns with a thickness of 38.67 nm. The d-spacing of 2.6 nm ZnO was observed with a bandgap of 2.7 eV. Multiple dyes were exposed to ZnO/N, S-CQDs photocatalyst. The MG decayed up to 72.8% in 180 min under the near-infrared region (NIR) and 85.4% in 60 mins in visible light. At the same time, ciprofloxacin (CIP) degrades under artificial sunlight in 20 min and under natural sunlight in 50 min, 92.9% and approximately, 85.8%respectively. MB photodegraded to 79% in 120 min in visible light. The designed photocatalyst was too exposed to Tianjin University Lake and Haihe River with different organic pollutants; the results were very attractive under sunlight irradiation. A wide range of photocatalytic activity is due to the reactive facets of ZnO in the 3-D nanostructure. The ability of nitrogen/ sulfur-doped carbon QDs of rapid electron transfer and upconverted luminescence. ZnO/N, S-CQDs have also degraded actual wastewater to decompose antibiotics up to 60% in 120 min under sunlight[150]. The nanoflowers combine ZnO nanosheets with facet $(10\bar{1}0)$ at the surface and higher oxygen vacancies. The electron trapping increase hence the reactive sites for the decay reaction. The hybrid shows sensitivity to a wide range of visible and near-infrared light due to the better upconverted luminescence property.

ZnO nanoflowers are a complex morphology of nanorods or nanosheets, and some grow out from the same nucleation point. The combined effects of multiple morphologies enhance the performance. The large surface area, reactive facets on the surface and higher defects ratio make them good candidate morphology. Multiple scattering is a unique attribute of the ZnO nanoflowers. The heterojunction and hybrid formation increases the absorption range much higher than any other ZnO nanostructure. Summary of 2D nanostructures and their photocatalytic performance is shown in Table 8 and 9.

## Advanced improvisation in nanostructures

Many different approaches are implied to synthesize new morphologies. Combining two or more dimensional nanostructures is created to enhance the performance. Hierarchical heterostructures have properties of different morphologies. A two-stage method implies novel ZnO nanoflowers combining ZnO nanorods and nanowires on polymer cores. The large surface area was achieved by combining two effective nanostructures, 1 D and 3 D. Controlled symmetry achieved by this approach opens new vistas for the application of photoactive and sensor applications[117,151].

Yang, C., et al., also attempted to decompose methylated dyes by synthesizing ZnO nanospheres. The control over the shape of NPs was attained by a two-stage method; later, the samples were annealed at various temperatures. The nanospheres annealed at 400 °C outperformed the others to degrade methylene blue by 99% in 70 minutes under UV irradiation. Better charge separation and redox potential is observed in the nanosphere due to the mesoporous surface with an average pore size of 15.5 nm. Band energy is also decreased to 3.1 eV from 3.3 eV with a diameter of 172 nm, and surface area increased to 43.9 $m^2g^{-1}$ [152,153]. The increased effective surface area due to the porous surface ascribes the effenciay to the photocatalyst. Tailoring in the bandgap energies allows better control over the absorption range of the material and redox reaction. Effective electron-hole separation is an attribute of efficient photocatalysis.

Zhu, Chengquan., et al., fabricated hollow spheres of ZnO by the facile method of size 450-1100 nm. RhB and reactive brilliant red K-2BP (BR K-2BP) were degraded in 135 and 120 min under UV spectra, respectively. The hollow spheres performed better than the commercial photocatalyst[154–156]. The light trapping is much more effective within the hollow sphere. Moreover, the porosity and increased surface area are responsible for photo decay. However, the diffusion rate of pollutants and intermediate is much less, negatively affecting performance.

ZnO nano-pellets were synthesized by Chiu, W., et al., using thermal pyrolysis. Later refluxing treatment was given to the samples. MB was photodegradation under UV light for 6 hours. The porous surface increases surface area up to 9.0687 $m^2g^{-1}$ with a pour size of 22.3342 nm. The recyclability was reported for up to 3 cycles. rate[157,158]. The increase in effenciay is due to the effective charge transport compared to the pristine ZnO without reflux. The photodegradation exposure time is very long.

Another ZnO 3-D comb is a combination of 2 D and 1 D nanostructures by Li, W., et al. the hydrothermal method gave 3-D comb developed by the growth of ZnO nanorods on

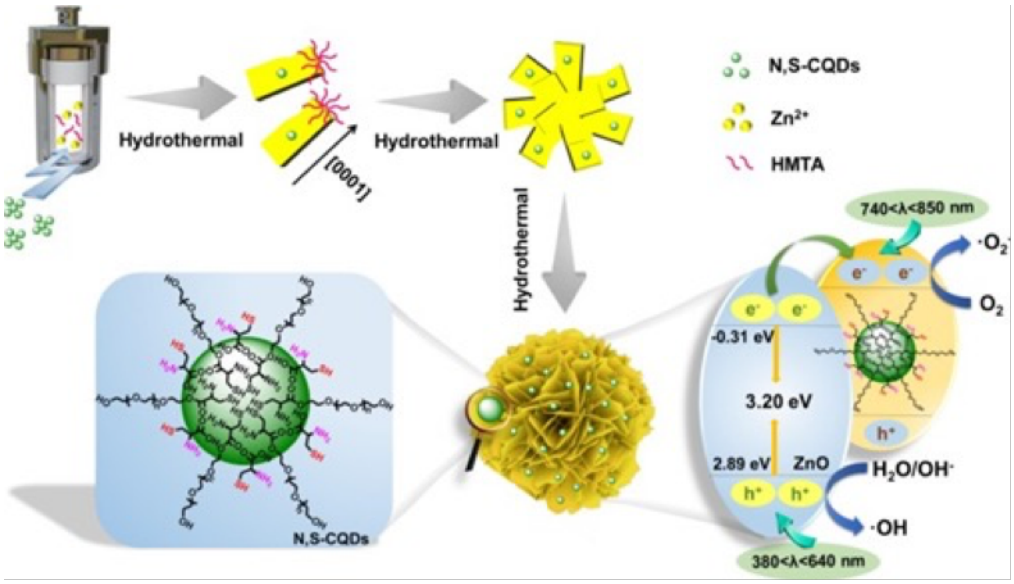


*Figure 20. Schematic of the synthesis of ZnO/N,S-CQDs nanoflowers* [150].

*Table 6. The Two-dimensional ZnO nanostructures*

| Improvi-sation | Method | a (A°) | c (A°) | Thickness (nm) | Surface area (m2g-1) | PL (nm) | Absorbance Peak (nm) | Band gap (eV) | Ref |
|---|---|---|---|---|---|---|---|---|---|
| ZnO | Solvothermal routes | 1.4 | 2.8 | 18 | - | ~590 | - | - | [143] |
| ZnO | Solvothermal annealing | 2.4 | 5.1 | 10-30 | 39.18 | 408 | - | - | [145] |
| ZnO/SnO | Hydrothermal | | | | | | 398 | | [146] |

*Table 7. The two-dimensional ZnO nanostructures and their performance*

| Improvisation | Wavelength range | Pollutant | % decay | Decay time (min) | Pollutant Dose (mg/liter) | Catalyst dose (mg/liter) | Reaction tempera-ture (°C) | Cycles | Ref |
|---|---|---|---|---|---|---|---|---|---|
| ZnO | UV-Visible | MB | 90% | 240 | 5 | - | RT | 3 | [143] |
| ZnO | UV | Phenol | 98% | 70 | 20 | 500 | RT | 4 | [145] |
| ZnO/SnO | Visible | MB | 90% | 6 | 10 | - | RT | 3 | [146] |

*Table 8. The three-dimensional ZnO nanostructures*

| Improvisation | Method | a (A°) | c (A°) | Thickness (nm) | Diameter (nm) | Surface area ($m^2g^{-1}$) | PL (nm) | Absorbance Peak (nm) | Band gap (eV) | Ref |
|---|---|---|---|---|---|---|---|---|---|---|
| ZnO | Low-temperature hydrothermal assisted route | 2.6 | - | 80-150 | 5000-6000 | - | 440-600 | - | - | [148] |
| | Microwave assisted growth | | - | 35.04 | 91 | 29.30 | 320 470 | 389 | 3.29 | [149] |
| ZnO/N,S-CQDs | One pot hydrother-mal | 2.6 | - | 38.67 | 1620 | - | 570 | >400 | 2.7 | [150] |

*Table 9. The three-dimensional ZnO nanostructures and their performance*

| Improvisation | Wavelength range | Pollutant | % decay | Decay time (min) | Pollutant Dose (mg/liter) | Catalyst dose (mg/liter) | Reaction temperature (°C) | Cycles | Ref |
|---|---|---|---|---|---|---|---|---|---|
| ZnO | UV | 4-CP | 80 % | 120 | 50 | - | RT | - | [148] |
| | Solar light | MB | 99% | 60 | 3 | 500 | RT | - | [149] |
| ZnO/N,S-CQDs | NIR | MG | 72.8% | 180 | | | | | |
| | Visible | | 85.4% | 60 | 7 | 400 | RT | 5 | [150] |
| | Visible | MB | 79% | 120 | | | | | |
| | Artificial sunlight | CIP | 92.9% | 20 | | | | | |
| | Natural sunlight | CIP | 85.8% | 50 | | | | | |
| | | Antibiotics | 40% | 120 | | | | | |

ZnO nanosheets. The diameter of 3-D combs was in the range of 3000-4000 nm. RhB exposed under Xe lamp for 1 hour for photodegradation up to 43%[159]. The double side comb combines nanorods and nanosheets with an enhanced surface-to-volume ratio. Multiple scattering of light and reactive sites on the surface are the attributes of the heterostructure. The large surface area increases the adsorption of organic dye to the surface and enables better diffusion; like hollow spheres, the 3-D combs have not shown better performance.

Kim, S., et al., synthesized nanocores by facet-selective etching method. The d spacing of reported ZnO nanocones is 0.28 nm with an average diameter of 10 nm. The RhB dye decays up to 95% in 80 minutes under the Xe lamp[160]. The nanostructure is unique, but the performance is limited to Xe Lamp wavelength.

The photocatalyst's major controlling factors are the higher surface-to-volume ratio, reduced recombination rates, and better diffusion of organic pollutants and polar facets. The better the control over the morphology, the better the effeciency of the catalyst will be. Summary of improvised nanostructures and their photocatalytic performance is shown in Table 10 and 11.

## FUTURE CHALLENGES AND PROSPECTS

The above review sums up the efforts of scientists to develop effective photocatalysts based on ZnO morphologies. Insight is given into the major factors and possible solutions to tune the ZnO nanostructures according to the photocatalytic application. Reducing the recombination rate, enhancing charge separation, and increased carrier life span on the surface are enhancing factors for photocatalytic reactions. The control overgrowth of polar facets, adsorption sites, increase in surface area and enhanced photon trapping directly influence the performance of the photocatalyst. The awareness of the newly engineered ZnO morphologies, heterojunction, heterostructure, nanocomposites, treasury hierarchical heterostructure and hybrid formation is crucial. Moreover, the effects of doping are effective in developing photocatalysts in the visible range.

The later oxidation decay of decorated material reduces the cyclic use of photocatalyst. The removal of catalyst and stability in the rectors are determining factors for commercial use. The heterostructure and nanocomposites must be cost-effective and stable. The combination of materials must be practically feasible for extensive use and eco-friendly. The removal of photocatalyst systems must improve as well. This review is mostly of the work in the late few years about the ZnO morphology based on photocatalytic activity for degradation of organic dyes. The presently reported work is very effective, but more improvements are required to achieve visible range active photocatalyst at room temperature. Consequently, the ZnO structural modifications (doping and coating with metals, heterojunction, hybrid and tertiary heterostructure formation) are required to activate a wide bandgap in the visible range for photon absorption.

Effective struggles are still needed to overcome the downsides of the laboratory photocatalyst. The photo decay of POPs must be exploited rather than probed organic dyes by research. The reactive rate of POPs is very difficult than the dyes. Extensive studies are required to investigate the degradation of organic pollutants such as pesticides, insecticides, antibiotics, and endocrine disrupting compounds. The ph variation, percentage concentration of pollutants and temperature for degradation reaction are various variables for different pollutants.

Moreover, the intermediates are not the same. Sometimes the AOP is required to remove the original pollutants. The surface reaction and kinematics of the intermediate and POPs

*Table 10. The improvised ZnO nanostructures*

| Improvisation | Method | a (A°) | c (A°) | Crystallite sizes (nm) | Diameter (nm) | Surface area ($m^2g^{-1}$) | PL (nm) | Band gap (eV) | Ref |
|---|---|---|---|---|---|---|---|---|---|
| Nanospheres | two stage solution | 2.5 | | 11.4 | 172 | 43.9 | 386 | 3.1 | [153] |
| Hollow Spheres | facile method | 3.25 | 5.21 | 6.1 | -450-1100 | 9.77 | - | - | [156] |
| Nano-pellets | thermal pyrolysis | - | - | - | 40-125 | 9.0687 | - | - | [158] |
| 3-D Comb | hydrothermal | - | - | - | 3000-4000 | - | - | - | [159] |
| Nanocores | facet-selective etching | 2.8 | - | - | 10 | - | 375 | - | [160] |

*Table 11. The improvised ZnO nanostructures and their performance*

| Improvisation | Active Wavelength | Pollutant | % decay | Decay time (min) | Pollutant Dose (mg/liter) | Catalyst dose (mg/liter) | Reaction temperature (°C) | Cycles | Ref |
|---|---|---|---|---|---|---|---|---|---|
| Nanospheres | UV | MB | 99% | 70 | 20 | 250 | RT | 5 | [153] |
| Hollow Spheres | UV | Rh B | 99% | 135 | 40 | 1000 | RT | - | [156] |
| | | BR K-2BP | | 120 | | | | | |
| Nano-pellets | UV light | MB | 94.9% | 360 | 5 | - | RT | 3 | [158] |
| 3-D Comb | Xe lamp | Rh B | 43% | 60 | - | - | - | - | [159] |
| Nanocores | Xe lamp | Rh B | 95% | 80 | 0.5 | 3 | RT | - | [160] |

varies widely, which is the major limiting factor of using a designed photocatalyst. A better understanding of the interface interaction of photocatalyst and pollutants can give the insight to develop photocatalytic nanostructure accordingly. Further work is needed in this regard.

The rectors are also a very important factor for the commercial application of designed nanostructures. The top choice of effective rectors and combination of photocatalyst with members in photocatalytic membrane reactors (PMR) is crucial. Many profound issues are present from fabrication, durability, stability of membranes, loss of catalyst from membranes and cost. Moreover, the operational issues such as leaching of the catalyst during treatment and recovery of catalyst post-treatment for cyclic use. The quantum yield, the kinetics of the reaction and optimum conditions are yet to be explored scientifically.

## CONCLUSIONS

In this review, numerous ZnO nanostructures were studied from the perspective of their photocatalytic application. It is observed that a slight variation in ZnO morphology affects physicochemical properties. Hence, they attribute it to the performance in photo activity. ZnO zero-dimension quantum dots and NPs hybrids exhibit better output in the photodegradation of POPs. Due to their higher surface area and reduced recombination rate. 1D nanostructures are reported to be more effective than 2D nanostructures. The lack in performance of 2D material is reduced due to multi-stacking despite the large surface area but ineffective surface area. It results in a lack of photon absorption, eventually reducing photocatalytic activity in 3D nanostructures showing adequate photocatalytic activity, same as near 1D nanostructures. 1D, 2D, and 3D nanostructures also have an issue with reproducibility. Hence 0D morphologies outperform the rest. Because of the large surface area, lack of recombination, high electron mobility, and higher photo absorption. The method of synthesis gets a bit tricky at nanoscale. Further investigations are still needed to study the development of ZnO-based nanostructures.

## References


1) Hartley, T. W. J. D. Public perception and participation in water reuse. *Desalination* **2006**, *187*, 115–126.
2) Bexell, M.; Jönsson, K. Responsibility and the United Nations' Sustainable Development Goals. *Forum for Development Studies* **2017**, *44* (1), 13–29.
3) Ghernaout, D. J. I. J. O. S. D. R. Water Reuse (WR): The Ultimate and Vital Solution for Water Supply Issues. *International Journal of Sustainable Development Research* **2017**, *3* (4), 36–36.
4) Van-Huy Nguyen,; Smith, S. M.; Wantala, K.; Kajitvichyanukul, P. Photocatalytic remediation of persistent organic pollutants (POPs): A review. *Arabian Journal of Chemistry* **2020**, *13* (11), 8309–8337.
5) Jones, K. C. J. E. S.; Technology, Persistent Organic Pollutants (POPs) and Related Chemicals in the Global Environment:

Some Personal Reflections. *Environmental Science & Technology* **2021**, *55* (14), 9400–9412.
6) Trojanowicz, M. J. S. O. T. T. E. Removal of persistent organic pollutants (POPs) from waters and wastewaters by the use of ionizing radiation. *Science of The Total Environment* **2020**, *718*, 134425–134425.
7) Pi, Y.; Li, X.; Xia, Q.; Wu, J.; Li, Y.; Xiao, J.; Li, Z. Adsorptive and photocatalytic removal of Persistent Organic Pollutants (POPs) in water by metal-organic frameworks (MOFs). *Chemical Engineering Journal* **2018**, *337*, 351–371.
8) Zhi, D.; Lin, Y.; Jiang, L.; Zhou, Y.; Huang, A.; Yang, J.; Luo, L. Remediation of persistent organic pollutants in aqueous systems by electrochemical activation of persulfates: A review. *Journal of Environmental Management* **2020**, *260*, 110125–110125.
9) Gaur, N.; Narasimhulu, K. Recent advances in the bio-remediation of persistent organic pollutants and its effect on environment. *Journal of Cleaner Production* **2018**, *198*, 1602–1631.
10) An, J.; Li, N.; Wang, S.; Liao, C.; Zhou, L.; Li, T.; Wang, X. A novel electrocoagulation-Fenton for energy efficient cyanobacteria and cyanotoxins removal without chemical addition. *Journal of hazardous materials* **2019**, *365*, 650–658.
11) Wang, J.; Wang, Z.; Vieira, C. L. Z.; Wolfson, J. M.; Pingtian, G.; Huang, S. Review on the treatment of organic pollutants in water by ultrasonic technology. *Ultrasonics Sonochemistry* **2019**, *55*, 273–278.
12) Kumari, P.; Bahadur, N.; Dumée, L. F. Photo-catalytic membrane reactors for the remediation of persistent organic pollutants – A review. *Separation and Purification Technology* **2020**, *230*, 115878–115878.
13) Varjani, S. J.; Gnansounou, E.; Pandey, A. J. C. Comprehensive review on toxicity of persistent organic pollutants from petroleum refinery waste and their degradation by microorganisms. *Chemosphere* **2017**, *188*, 280–291.
14) Tang, Y.; Rong, J.; Guan, X.; Zha, S.; Shi, W.; Han, Y.; Du, X.; Wu, F.; Huang, W.; Liu, G. Immunotoxicity of microplastics and two persistent organic pollutants alone or in combination to a bivalve species. *Environmental Pollution* **2020**, *258*, 113845–113845.
15) MM, M.; CA, M.; AK, K.; R, R. Recent trends in applications of advanced oxidation processes (AOPs) in bioenergy production. *Renewable and Sustainable Energy Reviews* **2020**, *121*, 109669–109669.
16) Kurt, A.; BK, M.; Ö, S.; T., Y. Treatment of antibiotics in wastewater using advanced oxidation processes (AOPs). Physico-chemical wastewater treatment and resource recovery. 2017.
17) Gil, A.; Galeano, L. A.; Vicente, M. A. In *Applications of advanced oxidation processes (AOPs) in drinking water treatment*; and others„ Ed.; Springer, 2019.
18) Bilotta, P.; Steinmetz, R. L. R.; Kunz, A.; Mores, R. Swine effluent post-treatment by alkaline control and UV radiation combined for water reuse. *Journal of Cleaner Production* **2017**, *140*, 1247–1254.
19) Ghernaout, D. Controlling Coagulation Process: From Zeta Potential to Streaming Potential. *American Journal of Environmental Protection* **2015**, *4* (5), 16–16.
20) Chang, J.; Lee, W.; Yoon, S. J. J. O. C. P. Energy consumptions and associated greenhouse gas emissions in operation phases of urban water reuse systems in Korea. *Journal of Cleaner Production* **2017**, *141*, 728–736.
21) Chen, D.; Cheng, Y.; Zhou, N.; Chen, P.; Wang, Y.; Li, K.; Huo, S.; Cheng, P.; Peng, P.; Zhang, R.; Wang, L.; Liu, H.; Liu, Y.; Ruan, R. Photocatalytic degradation of organic pollutants using TiO2-based photocatalysts: A review. *Journal of Cleaner Production* **2020**, *268*, 121725–121725.
22) Naeem, H. M.; Tariq, S.; Moiz, M. A.; Khan, M.; Rehman, N.; Basit, M. A. Activating ZnO-Based Hierarchical Particles for Visible Light Dependent Photocatalytic Performance via Cr-Incorporated Rapid Chemical Synthesis. *Crystal Research and Technology* **2022**, *57* (3), 2100125–2100125.
23) Moiz, M. A.; Mumtaz, A.; Salman, M.; Mazhar, H.; Basit, M. A.; Husain, S. W.; Ramzan, M. Enhancement of Dye Degradation by Zinc Oxide via Transition-Metal Doping: A Review. *Journal of Electronic Materials* **2021**, *50* (9), 5106–5121.
24) Khan, T. F.; Muhyuddin, M.; Husain, S. W.; Basit, M. A. Synthesis and Characterization of ZnO-ZnS Nanoflowers for Enhanced Photocatalytic Performance : ZnS Decorated ZnO Nanoflowers. *2019 16th International Bhurban Conference on Applied Sciences and Technology (IBCAST)* **2019**,
25) Ahmad, W.; Basit, M. A.; Khan, M. S.; Ali, I.; Park, T. J. Superior atomic layer deposition of conformal ZnO shell on spherical SiO2 particles for enhanced photocatalytic activity. *Physica E: Low-dimensional Systems and Nanostructures* **2020**, *124*, 114308–114308.
26) Khan, M.; Irfan, M. H.; Israr, M.; Rehman, N.; Park, T. J.; Basit, M. A. Comparative investigation of ZnO morphologies for optimal CdS quantum-dot deposition via pseudo-SILAR method. *Chemical Physics Letters* **2020**, *744*, 137223–137223.
27) Naeem, H. M.; Ijaz, S.; Abbas, M. H.; Ahmed, Y.; Rehman, N.; Park, T. J.; Basit, M. A. HF-based surface modification for enhanced photobiological and photochemical performance of ZnO and ZnO/CdS hierarchical structures. *Materials Chemistry and Physics* **2020**, *252*, 123190–123190.
28) Fukuzumi, S.; Lee, Y.-M.; Nam, W. J. C. C. R. Thermal and photocatalytic production of hydrogen with earth-abundant metal complexes. *Coordination Chemistry Reviews* **2018**, *355*, 54–73.
29) Qi, K.; Cheng, B.; Yu, J.; Ho, W. Review on the improvement of the photocatalytic and antibacterial activities of ZnO. *Journal of Alloys and Compounds* **2017**, *727*, 792–820.
30) Zhang, C.; Gu, Y.; Teng, G.; Wang, L.; Jin, X.; Qiang, Z.; Ma, W. Fabrication of a Double-Shell Ag/AgCl/G-ZnFe<sub>2</sub>O<sub>4</sub> Nanocube with Enhanced Light Absorption and Superior Photocatalytic Antibacterial Activity. *ACS Applied Materials & Interfaces* **2020**, *12* (26), 29883–29898.
31) Ren, H.; Koshy, P.; Chen, W.-F.; Qi, S.; Sorrell, C. C. Photocatalytic materials and technologies for air purification. *Journal of Hazardous Materials* **2017**, *325*, 340–366.
32) Yuan, J.; Yi, X.; Tang, Y.; Liu, M.; Liu, C. Efficient Photocatalytic Nitrogen Fixation: Enhanced Polarization, Activation, and Cleavage by Asymmetrical Electron Donation to N≡N Bond. *Advanced Functional Materials* **2020**, *30* (4), 1906983–1906983.
33) Natarajan, S.; Bajaj, H. C.; Tayade, R. J. Recent advances based on the synergetic effect of adsorption for removal of dyes from waste water using photocatalytic process. *Journal of Environmental Sciences* **2018**, *65*, 201–222.
34) Brillas, E.; Martínez-Huitle, C. A. Decontamination of wastewaters containing synthetic organic dyes by electrochemical methods. An updated review. *Applied Catalysis B: Environmental* **2015**, *166-167*, 603–643.
35) Wang, K. H.; Tsai, H.; Hsieh, Y.-H. J. C. A study of photocatalytic degradation of trichloroethylene in vapor phase on TiO2 photocatalyst. *Chemosphere* **1998**, *36*, 2763–2773.
36) Malato, S.; Blanco, J.; Cáceres, J.; Fernández-Alba, A. R.; Agüera, A.; Rodríguez, A. Photocatalytic treatment of water-soluble pesticides by photo-Fenton and TiO2 using solar energy. *Catalysis Today* **2002**, *76* (2-4), 209–220.
37) Xekoukoulotakis, N. P.; Xinidis, N.; Chroni, M.; Mantzavinos, D.; Venieri, D.; Hapeshi, E.; Fatta-Kassinos, D. UV-A/TiO2 photocatalytic decomposition of erythromycin in water: Factors affecting mineralization and antibiotic activity. *Catalysis Today* **2010**, *151* (1-2), 29–33.
38) Nakano, K.; Obuchi, E.; Takagi, S.; Yamamoto, R.; Tanizaki, T.; Taketomi, M.; Eguchi, M.; Ichida, K.; Suzuki, M.; Hashimoto, A. Photocatalytic treatment of water containing dinitrophenol and city water over TiO2/SiO2. *Separation and Purification Technology* **2004**, *34* (1-3), 67–72.

39) Bamba, D.; Coulibaly, M.; Robert, D. J. S. O. T. T. E. Nitrogen-containing organic compounds: Origins, toxicity and conditions of their photocatalytic mineralization over TiO2. *Science of The Total Environment* **2017**, *580*, 1489–1504.
40) Fatima, R.; Kim, J.-O. J. A. S. S. Inhibiting photocatalytic electron-hole recombination by coupling MIL-125(Ti) with chemically reduced, nitrogen-containing graphene oxide. *Applied Surface Science* **2021**, *541*, 148503–148503.
41) Fernandes, A.; Gągol, M.; Makoś, P.; Khan, J. A.; Boczkaj, G. Integrated photocatalytic advanced oxidation system (TiO2/UV/O3/H2O2) for degradation of volatile organic compounds. *Separation and Purification Technology* **2019**, *224*, 1–14.
42) Selishchev, D. S.; Kolobov, N. S.; Pershin, A. A.; Kozlov, D. V. TiO2 mediated photocatalytic oxidation of volatile organic compounds: Formation of CO as a harmful by-product. *Applied Catalysis B: Environmental* **2017**, *200*, 503–513.
43) Bai, H.; Zhou, J.; Zhang, H.; Tang, G. Enhanced adsorbability and photocatalytic activity of TiO 2 -graphene composite for polycyclic aromatic hydrocarbons removal in aqueous phase. *Colloids and Surfaces B: Biointerfaces* **2017**, *150*, 68–77.
44) Van-Huy Nguyen,; Thi, L.-A. P.; Le, Q. V.; Singh, P.; Raizada, P.; Kajitvichyanukul, P. Tailored photocatalysts and revealed reaction pathways for photodegradation of polycyclic aromatic hydrocarbons (PAHs) in water, soil and other sources. *Chemosphere* **2020**, *260*, 127529–127529.
45) Yang, X.; Cai, H.; Bao, M.; Yu, J.; Lu, J.; Li, Y. Highly Efficient Photocatalytic Remediation of Simulated Polycyclic Aromatic Hydrocarbons (PAHs) Contaminated Wastewater under Visible Light Irradiation by Graphene Oxide Enwrapped Ag<sub>3</sub>PO<sub>4</sub>Composite. *Chinese Journal of Chemistry* **2017**, *35* (10), 1549–1558.
46) Al-Madanat, O.; Alsalka, Y.; Ramadan, W.; Bahnemann, D. W. TiO2 Photocatalysis for the Transformation of Aromatic Water Pollutants into Fuels. *Catalysts* **2021**, *11* (3), 317–317.
47) Stoyanova, A.; Bachvarova-Nedelcheva, A.; Iordanova, R. J. J. C. T. M. Photocatalytic degradation of two azo-dyes in single and binary mixture by La modified TiO2. *Journal of Chemical Technology and Metallurgy* **2018**, *53*, 1173–1178.
48) Iga, G. D.; Peixoto, A. L. D. C.; Costalonga, A. G. C. Efficient Optimization of Photocatalytic Process for Azo Dyes. *Proceedings of the 4th Brazilian Technology Symposium (BTSym'18)* **2019**, 313–317.
49) Álvaro Pérez-Molina,; Morales-Torres, S.; Maldonado-Hódar, F.; Pastrana-Martínez, L. Functionalized Graphene Derivatives and TiO2 for High Visible Light Photodegradation of Azo Dyes. *Nanomaterials* **2020**, *10* (6), 1106–1106.
50) Wang, A.; Teng, Y.; Hu, X.-F.; Wu, L.-H.; Huang, Y.-J.; Luo, Y.-M.; Christie, P. Diphenylarsinic acid contaminated soil remediation by titanium dioxide (P25) photocatalysis: Degradation pathway, optimization of operating parameters and effects of soil properties. *Science of The Total Environment* **2016**, *541*, 348–355.
51) Swarnakar, P.; Kanel, S. R.; Nepal, D.; Jiang, Y.; Jia, H.; Kerr, L.; Goltz, M. N.; Levy, J.; Rakovan, J. Silver deposited titanium dioxide thin film for photocatalysis of organic compounds using natural light. *Solar Energy* **2013**, *88*, 242–249.
52) Rapsomanikis, A.; Apostolopoulou, A.; Stathatos, E.; Lianos, P. Cerium-modified TiO2 nanocrystalline films for visible light photocatalytic activity. *Journal of Photochemistry and Photobiology A: Chemistry* **2014**, *280*, 46–53.
53) Choi, J.; Park, H.; Hoffmann, M. R. Effects of Single Metal-Ion Doping on the Visible-Light Photoreactivity of TiO<sub>2</sub>. *The Journal of Physical Chemistry C* **2010**, *114* (2), 783–792.
54) Bhattacharyya, K.; Majeed, J.; Dey, K. K.; Ayyub, P.; Tyagi, A. K.; Bharadwaj, S. R. Effect of Mo-Incorporation in the TiO<sub>2</sub> Lattice: A Mechanistic Basis for Photocatalytic Dye Degradation. *The Journal of Physical Chemistry C* **2014**, *118* (29), 15946–15962.
55) Sornalingam, K.; Mcdonagh, A.; Zhou, J. L.; Johir, M. A. H.; Ahmed, M. B. Photocatalysis of estrone in water and wastewater: Comparison between Au-TiO2 nanocomposite and TiO2, and degradation by-products. *Science of The Total Environment* **2018**, *610-611*, 521–530.
56) Nasir, M.; Bagwasi, S.; Jiao, Y.; Chen, F.; Tian, B.; Zhang, J. Characterization and activity of the Ce and N co-doped TiO 2 prepared through hydrothermal method. *Chemical Engineering Journal* **2014**, *236*, 388–397.
57) Bagwasi, S.; Tian, B.; Zhang, J.; Nasir, M. Synthesis, characterization and application of bismuth and boron Co-doped TiO2: A visible light active photocatalyst. *Chemical Engineering Journal* **2013**, *217*, 108–118.
58) Kaviyarasu, K.; Mariappan, A.; Neyvasagam, K.; Ayeshamariam, A.; Pandi, P.; Palanichamy, R. R.; Gopinathan, C.; Mola, G. T.; Maaza, M. Photocatalytic performance and antimicrobial activities of HAp-TiO2 nanocomposite thin films by sol-gel method. *Surfaces and Interfaces* **2017**, *6*, 247–255.
59) Karthikeyan, K. T.; Nithya, A.; Jothivenkatachalam, K. Photocatalytic and antimicrobial activities of chitosan-TiO2 nanocomposite. *International Journal of Biological Macromolecules* **2017**, *104*, 1762–1773.
60) Santhosh, C.; Malathi, A.; Daneshvar, E.; Kollu, P.; Bhatnagar, A. Photocatalytic degradation of toxic aquatic pollutants by novel magnetic 3D-TiO2@HPGA nanocomposite. *Scientific Reports* **2018**, *8* (1), 1–15.
61) Bhanvase, B. A.; Shende, T. P.; Sonawane, S. H. A review on graphene–TiO<sub>2</sub> and doped graphene–TiO<sub>2</sub> nanocomposite photocatalyst for water and wastewater treatment. *Environmental Technology Reviews* **2017**, *6* (1), 1–14.
62) Sun, X.; Yan, L.; Xu, R.; Xu, M.; Zhu, Y. Surface modification of TiO2 with polydopamine and its effect on photocatalytic degradation mechanism. *Colloids and Surfaces A: Physicochemical and Engineering Aspects* **2019**, *570*, 199–209.
63) Zong, H.; Zhao, T.; Zhou, G.; Qian, R.; Feng, T.; Pan, J. H. Revisiting structural and photocatalytic properties of g-C3N4/TiO2: Is surface modification of TiO2 by calcination with urea an effective route to "solar" photocatalyst? *Catalysis Today* **2019**, *335*, 252–261.
64) Cha, B. J.; Saqlain, S.; Seo, H. O.; Kim, Y. D. Hydrophilic surface modification of TiO2 to produce a highly sustainable photocatalyst for outdoor air purification. *Applied Surface Science* **2019**, *479*, 31–38.
65) Sharma, P. K.; Cortes, M. A. L. R. M.; Hamilton, J. W. J.; Han, Y.; Byrne, J. A.; Nolan, M. Surface modification of TiO2 with copper clusters for band gap narrowing. *Catalysis Today* **2019**, *321-322*, 9–17.
66) Moloto, N.; Mpelane, S.; Sikhwivhilu, L. M.; Ray, S. S. Optical and Morphological Properties of ZnO and TiO2 Derived Nanostructures Synthesized via a Microwave-Assisted Hydrothermal Method. *Advances in Energy Research* **2020**,
67) Khan, M. E.; Khan, M. M.; Cho, M. H. Recent progress of metal–graphene nanostructures in photocatalysis. *Nanoscale* **1920**, *10* (20), 9427–9440.
68) Ihnatiuk, D. Sunlight-driven photocatalytic reduction of noble metals ions to nanoparticles. 2019.
69) Allen, N. S.; Mahdjoub, N.; Vishnyakov, V.; Kelly, P. J.; Kriek, R. J. The effect of crystalline phase (anatase, brookite and rutile) and size on the photocatalytic activity of calcined polymorphic titanium dioxide (TiO 2 ). *Polymer Degradation and Stability* **2018**, *150*, 31–36.
70) Subhan, M. A.; Saha, P. C.; Sumon, S. A.; Ahmed, J.; Asiri, A. M.; Rahman, M. M.; Al-Mamun, M. Enhanced photocatalytic activity and ultra-sensitive benzaldehyde sensing performance of a SnO<sub>2</sub>·ZnO·TiO<sub>2</sub> nanomaterial. *RSC Advances* **2018**, *8* (58), 33048–33058.
71) Ong, C. B.; Ng, L. Y.; Mohammad, A. W. A review of ZnO nanoparticles as solar photocatalysts: Synthesis, mechanisms and

applications. *Renewable and Sustainable Energy Reviews* **2018**, *81*, 536–551.
72) Feng, C.; Chen, Z.; Jing, J.; Hou, J. The photocatalytic phenol degradation mechanism of Ag-modified ZnO nanorods. *Journal of Materials Chemistry C* **2020**, *8* (9), 3000–3009.
73) Chang, J. S.; Strunk, J.; Chong, M. N.; Poh, P. E.; Ocon, J. D. Multi-dimensional zinc oxide (ZnO) nanoarchitectures as efficient photocatalysts: What is the fundamental factor that determines photoactivity in ZnO? *Journal of Hazardous Materials* **2020**, *381*, 120958–120958.
74) Mufti, N.; Laila, I. K. R.; Idiawati, R.; Fuad, A.; Hidayat, A.; Taufiq, A.; Sunaryono, The Effect of Growth Temperature on The Characteristics Of ZnO Nanorods And Its Optical Properties. *Journal of Physics: Conference Series* **2018**, *1057*, 012005–012005.
75) Chen, X.; Wu, Z.; Liu, D.; Gao, Z. Preparation of ZnO Photocatalyst for the Efficient and Rapid Photocatalytic Degradation of Azo Dyes. *Nanoscale Research Letters* **2017**, *12* (1), 1–10.
76) Liang, S.; Xiao, K.; Mo, Y.; Huang, X. A novel ZnO nanoparticle blended polyvinylidene fluoride membrane for anti-irreversible fouling. *Journal of Membrane Science* **2012**, *394-395*, 184–192.
77) Zailan, S. N.; Bouaissi, A.; Mahmed, N.; Abdullah, M. M. A. B. Influence of ZnO Nanoparticles on Mechanical Properties and Photocatalytic Activity of Self-cleaning ZnO-Based Geopolymer Paste. *Journal of Inorganic and Organometallic Polymers and Materials* **2020**, *30* (6), 2007–2016.
78) Kaddes, M.; Omri, K.; Kouaydi, N.; Zemzemi, M. Structural, electrical and optical properties of ZnO nanoparticle: combined experimental and theoretical study. *Applied Physics A* **2018**, *124* (8), 1–7.
79) Barzinjy, A. A. Structure, synthesis and applications of ZnO nanoparticles: A review. *Jordan Journal of Physics* **2020**, *13*, 123–135.
80) Mauro, A. D.; Fragala, M. E.; Privitera, V.; Impellizzeri, G. ZnO for application in photocatalysis: From thin films to nanostructures . *Materials Science in Semiconductor Processing* **2017**, *69*, 44–51.
81) Borysiewicz, M. A. J. C. ZnO as a Functional Material, a Review. *Crystals* **2019**, *9* (10), 505–505.
82) Theerthagiri, J.; Salla, S.; Senthil, R. A.; Nithyadharseni, P.; Madankumar, A.; Arunachalam, P.; Maiyalagan, T.; Kim, H.-S. A review on ZnO nanostructured materials: energy, environmental and biological applications. *Nanotechnology* **2019**, *30* (39), 392001–392001.
83) Basit, M.; N, S.; S, A.; A, Z. Cobalt doping effects on zinc oxide transparent conducting thin films. *World Applied Sciences Journal* **2014**, *32*, 1664–1670.
84) Zia, A.; Ahmed, S.; Shah, N. A.; Anis-Ur-Rehman, M.; Khan, E. U.; Basit, M. Consequence of cobalt on structural, optical and dielectric properties in ZnO nanostructures. *Physica B: Condensed Matter* **2015**, *473*, 42–47.
85) Harun, K.; Hussain, F.; Purwanto, A.; Sahraoui, B.; Zawadzka, A.; Mohamad, A. A. Sol–gel synthesized ZnO for optoelectronics applications: a characterization review. *Materials Research Express* **2017**, *4* (12), 122001–122001.
86) Ortiz-Casas, B.; Galdámez-Martínez, A.; Gutiérrez-Flores, J.; Ibañez, A. B.; Panda, P. K.; Santana, G.; Vega, H. A. D. L.; Suar, M.; Rodelo, C. G.; Kaushik, A.; Mishra, Y. K.; Dutt, A. Bio-acceptable 0D and 1D ZnO nanostructures for cancer diagnostics and treatment. *Materials Today* **2021**, *50*, 533–569.
87) Kang, Y.; Yu, F.; Zhang, L.; Wang, W.; Chen, L.; Li, Y. Review of ZnO-based nanomaterials in gas sensors. *Solid State Ionics* **2021**, *360*, 115544–115544.
88) Basit, M.; Abbas, M.; Ahmad, N.; Javed, S.; Shah, N. A. Synthesis of ZnO/CNT Nanocomposites for Ultraviolet Sensors. 2022. 9. *Frontiers in Materials* **2022**, *9*.
89) Kwon, D.-K.; Porte, Y.; Ko, K. Y.; Kim, H.; Myoung, J.-M. High-Performance Flexible ZnO Nanorod UV/Gas Dual Sensors Using Ag Nanoparticle Templates. *ACS Applied Materials & Interfaces* **2018**, *10* (37), 31505–31514.
90) Roy, A.; Mead, J.; Wang, S.; Huang, H. Effects of surface defects on the mechanical properties of ZnO nanowires. *Scientific Reports* **2017**, *7* (1), 1–8.
91) Malakooti, M. H.; Hwang, H.-S.; Goulbourne, N. C.; Sodano, H. A. Role of ZnO nanowire arrays on the impact response of aramid fabrics. *Composites Part B: Engineering* **2017**, *127*, 222–231.
92) Mohamed, W. A. A.; El-Gawad, H. H. A.; Mekkey, S. D.; Galal, H. R.; Labib, A. A. Zinc oxide quantum dots: Confinement size, photophysical and tunning optical properties effect on photodecontamination of industrial organic pollutants. *Optical Materials* **2021**, *118*, 111242–111242.
93) Sowik, J.; Miodyńska, M.; Bajorowicz, B.; Mikolajczyk, A.; Lisowski, W.; Klimczuk, T.; Kaczor, D.; Medynska, A. Z.; Malankowska, A. Optical and photocatalytic properties of rare earth metal-modified ZnO quantum dots. *Applied Surface Science* **2019**, *464*, 651–663.
94) Vattikuti, S. V. P.; Reddy, P. A. K.; Shim, J.; Byon, C. Visible-Light-Driven Photocatalytic Activity of SnO2-ZnO Quantum Dots Anchored on g-C3N4 Nanosheets for Photocatalytic Pollutant Degradation and H2 Production. *ACS Omega* **2018**, *3* (7), 7587–7602.
95) Ali, S.; Razzaq, A.; Kim, H.; In, S.-I. Activity, selectivity, and stability of earth-abundant CuO/Cu2O/Cu0-based photocatalysts toward CO2 reduction. *Chemical Engineering Journal* **2022**, *429*, 131579–131579.
96) Anitha, S.; Balu, A. R.; Balamurugan, S.; Suganya, M.; Delci, Z.; Karthika, M.; Kayathiri, C.; Devi, S. C. A comparative study on the photocatalytic performance of two third order NLO active nanocomposites (NiO-CdO and NiO-CuO) green synthesized using Psidium guajava leaf extract. *Inorganic Chemistry Communications* **2021**, *134*, 109073–109073.
97) Raizada, P.; Sudhaik, A.; Patial, S.; Hasija, V.; Khan, A. A. P.; Singh, P.; Gautam, S.; Kaur, M.; Van-Huy Nguyen, Engineering nanostructures of CuO-based photocatalysts for water treatment: Current progress and future challenges. *Arabian Journal of Chemistry* **2020**, *13* (11), 8424–8457.
98) Fakhri, A.; Azad, M.; Tahami, S. J. J. O. M. S. M. I. E. Degradation of toxin via ultraviolet and sunlight photocatalysis using ZnO quantum dots/CuO nanosheets composites: preparation and characterization studies. *Journal of Materials Science: Materials in Electronics* **2017**, *28* (21), 16397–16402.
99) Kumar, K. V. A.; Lakshminarayana, B.; Suryakala, D.; Subrahmanyam, C. H. Reduced graphene oxide supported ZnO quantum dots for visible light-induced simultaneous removal of tetracycline and hexavalent chromium. *RSC Advances* **2020**, *10* (35), 20494–20503.
100) Wang, X.; Li, J. J. O. M. Sol-gel fabrication of Ag-Coated ZnO quantum dots nanocomposites with excellent photocatalytic activity. *Optical Materials* **2021**, *118*, 111235–111235.
101) Fakhri, A.; Azad, M.; Fatolahi, L.; Tahami, S. Microwave-assisted photocatalysis of neurotoxin compounds using metal oxides quantum dots/nanosheets composites: Photocorrosion inhibition, reusability and antibacterial activity studies. *Journal of Photochemistry and Photobiology B: Biology* **2018**, *178*, 108–114.
102) Zhou, Q.; Li, L.; Zhang, X.; Yang, H.; Cheng, Y.; Che, H.; Wang, L.; Cao, Y. Construction of heterojunction and homojunction to improve the photocatalytic performance of ZnO quantum dots sensitization three-dimensional ordered hollow sphere ZrO2–TiO2 arrays. *International Journal of Hydrogen Energy* **2020**, *45* (56), 31812–31824.
103) Iqbal, A.; Saidu, U.; Adam, F.; Sreekantan, S.; Jasni, N.; Ahmad, M. N. The Effects of Zinc Oxide (ZnO) Quantum Dots (QDs) Embedment on the Physicochemical Properties and Photocatalytic Activity of Titanium Dioxide (TiO2) Nanoparticles. *Journal of Physical Science* **2021**, *32* (2), 71–85.
104) Mahdavi, R.; Talesh, S. S. A. The effect of ultrasonic irradiation on the struc-

ture, morphology and photocatalytic performance of ZnO nanoparticles by sol-gel method. *Ultrasonics Sonochemistry* **2017**, *39*, 504–510.
105) Ghaderi, A.; Abbasi, S.; Farahbod, F. J. M. R. E. Synthesis, characterization and photocatalytic performance of modified ZnO nanoparticles with SnO<sub>2</sub> nanoparticles. *Materials Research Express* **2018**, *5* (6), 065908–065908.
106) Ghaderi, A.; Abbasi, S.; Farahbod, F. J. I. J. O. C. E. 2015.
107) Mahdavi, R.; Talesh, S. S. A. Sol-gel synthesis, structural and enhanced photocatalytic performance of Al doped ZnO nanoparticles. *Advanced Powder Technology* **2017**, *28* (5), 1418–1425.
108) Zhang, X.; Chen, Y.; Zhang, S.; Qiu, C. High photocatalytic performance of high concentration Al-doped ZnO nanoparticles. *Separation and Purification Technology* **2017**, *172*, 236–241.
109) Lopes, J. L.; Martins, M. J.; Nogueira, H. I. S.; Estrada, A. C.; Trindade, T. Carbon-based heterogeneous photocatalysts for water cleaning technologies: a review. *Environmental Chemistry Letters* **2021**, *19* (1), 643–668.
110) Liang, H.; Tai, X.; Du, Z.; Yin, Y. Enhanced photocatalytic activity of ZnO sensitized by carbon quantum dots and application in phenol wastewater. *Optical Materials* **2020**, *100*, 109674–109674.
111) Boppella, R.; Anjaneyulu, K.; Basak, P.; Manorama, S. V. Facile Synthesis of Face Oriented ZnO Crystals: Tunable Polar Facets and Shape Induced Enhanced Photocatalytic Performance. *The Journal of Physical Chemistry C* **2013**, *117* (9), 4597–4605.
112) Pruna, A.; Wu, Z.; Zapien, J. A.; Li, Y. Y.; Ruotolo, A. Enhanced photocatalytic performance of ZnO nanostructures by electrochemical hybridization with graphene oxide. *Applied Surface Science* **2018**, *441*, 936–944.
113) Rosli, N. I. M.; Lam, S.-M.; Sin, J.-C.; Satoshi, I.; Mohamed, A. R. Photocatalytic Performance of ZnO/g-C3N4 for Removal of Phenol under Simulated Sunlight Irradiation. *Journal of Environmental Engineering* **2018**, *144* (2), 4017091–4017091.
114) Faraz, M.; Naqvi, F. K.; Shakir, M.; Khare, N. Synthesis of samarium-doped zinc oxide nanoparticles with improved photocatalytic performance and recyclability under visible light irradiation. *New Journal of Chemistry* **2018**, *42* (3), 2295–2305.
115) Araujo, F. P.; Trigueiro, P.; Honório, L. M. C.; Furtini, M. B.; Oliveira, D. M.; Almeida, L. C.; Garcia, R. R. P.; Viana, B. C.; Silva-Filho, E. C.; Osajima, J. A. A novel green approach based on ZnO nanoparticles and polysaccharides for photocatalytic performance. *Dalton Transactions* **2020**, *49* (45), 16394–16403.
116) Samadi, M.; Zirak, M.; Naseri, A.; Kheirabadi, M.; Ebrahimi, M.; Moshfegh, A. Z. Design and tailoring of one-dimensional ZnO nanomaterials for photocatalytic degradation of organic dyes: a review. *Research on Chemical Intermediates* **2019**, *45* (4), 2197–2254.
117) Zhang, X.; Qin, J.; Xue, Y.; Yu, P.; Zhang, B.; Wang, L.; Liu, R. Effect of aspect ratio and surface defects on the photocatalytic activity of ZnO nanorods. *Scientific Reports* **2015**, *4* (1), 1–8.
118) Sun, T.; Qiu, J.; Liang, C. J. T. J. O. P. C. C. Controllable Fabrication and Photocatalytic Activity of ZnO Nanobelt Arrays. *The Journal of Physical Chemistry C* **2008**, *112* (3), 715–721.
119) Wang, M.; Fei, G. T.; Zhang, L. J. N. Porous-ZnO-Nanobelt Film as Recyclable Photocatalysts with Enhanced Photocatalytic Activity. *Nanoscale Research Letters* **2010**, *5* (11), 1800–1803.
120) Das, A.; S.K., N.; Nair, R. G. Influence of surface morphology on photocatalytic performance of zinc oxide: A review. *Nano-Structures & Nano-Objects* **2019**, *19*, 100353–100353.
121) Li, X.; Li, X.; Zhu, B.; Lang, J.; Chen, X. Synthesis of ZnSe/ZnO Nanobelts for Enhanced Visible Light Photocatalytic Activity. *Science of Advanced Materials* **2018**, *10* (9), 1320–1326.
122) Fauzi, A. A.; Jalil, A. A.; Hassan, N. S.; Aziz, F. F. A.; Azami, M. S.; Hussain, I.; Saravanan, R.; Vo, D. A critical review on relationship of CeO2-based photocatalyst towards mechanistic degradation of organic pollutant. *Chemosphere* **2022**, *286*, 131651–131651.
123) Li, Q. *A Review on Ceo2-Based Electrocatalyst and Photocatalyst in Energy Conversion. 2021 2* (2), 2000063–2000063.
124) Rajendran, S.; Khan, M. M.; Gracia, F.; Qin, J.; Gupta, V. K.; Arumainathan, S. Ce3+-ion-induced visible-light photocatalytic degradation and electrochemical activity of ZnO/CeO2 nanocomposite. *Scientific Reports* **2016**, *6* (1), 1–11.
125) Das, A.; Patra, M.; P, M. K.; Bhagavathiachari, M.; Nair, R. G. Defect-induced visible-light-driven photocatalytic and photoelectrochemical performance of ZnO–CeO2 nanoheterojunctions. *Journal of Alloys and Compounds* **2021**, *858*, 157730–157730.
126) Saravanan, R.; Karthikeyan, N.; Govindan, S.; Narayanan, V.; Stephen, A. Photocatalytic Degradation of Organic Dyes Using ZnO/CeO<sub>2</sub> Nanocomposite Material under Visible Light. *Advanced Materials Research* **2012**, *584*, 381–385.
127) Zhang, Q.; Ma, Q.; Guo, J.; Li, H.; Wang, Y.; Wang, X. Surface oxygen vacancies modified ridge-like CeO2/ZnO nanobelts for enhancing photocatalytic activity. *Chemical Physics Letters* **2022**, *791*, 139376–139376.
128) Fu, D.; Han, G.; Meng, C. J. M. L. Size-controlled synthesis and photocatalytic degradation properties of nano-sized ZnO nanorods. *Materials Letters* **2012**, *72*, 53–56.
129) Sadaiyandi, K. Influence of Mg doping on ZnO nanoparticles for enhanced photocatalytic evaluation and antibacterial analysis. *Nanoscale Research Letters* **2018**, *13*, 1–13.
130) Hsu, M.-H.; Chang, C.-J. J. J. Ag-doped ZnO nanorods coated metal wire meshes as hierarchical photocatalysts with high visible-light driven photoactivity and photostability. *Journal of Hazardous Materials* **2014**, *278*, 444–453.
131) Shen, R.; Jiang, C.; Xiang, Q.; Xie, J.; Li, X. Surface and interface engineering of hierarchical photocatalysts. *Applied Surface Science* **2019**, *471*, 43–87.
132) Sin, J.-C.; Lam, S.-M.; Lee, K.-T.; Mohamed, A. R. Preparation and photocatalytic properties of visible light-driven samarium-doped ZnO nanorods. *Ceramics International* **2013**, *39* (5), 5833–5843.
133) Kumar, S.; Dhiman, A.; Sudhagar, P.; Krishnan, V. ZnO-graphene quantum dots heterojunctions for natural sunlight-driven photocatalytic environmental remediation. *Applied Surface Science* **2018**, *447*, 802–815.
134) Xu, T.; Hu, J.; Yang, Y.; Que, W.; Yin, X.; Wu, H.; Chen, L. Ternary system of ZnO nanorods/reduced graphene oxide/CuInS2 quantum dots for enhanced photocatalytic performance. *Journal of Alloys and Compounds* **2018**, *734*, 196–203.
135) Lee, K. M.; Lai, C. W.; Ngai, K. S.; Juan, J. C. Recent developments of zinc oxide based photocatalyst in water treatment technology: A review. *Water Research* **2016**, *88*, 428–448.
136) Liu, Y.; Kang, Z. H.; Chen, Z. H.; Shafiq, I.; Zapien, J. A.; Bello, I.; Zhang, W. J.; Lee, S. T. Synthesis, Characterization, and Photocatalytic Application of Different ZnO Nanostructures in Array Configurations. *Crystal Growth & Design* **2009**, *9* (7), 3222–3227.
137) Udom, I.; Zhang, Y.; Ram, M. K.; Stefanakos, E. K.; Hepp, A. F.; Elzein, R.; Schlaf, R.; Goswami, D. Y. A simple photolytic reactor employing Ag-doped ZnO nanowires for water purification. *Thin Solid Films* **2014**, *564*, 258–263.
138) Ebrahimi, M.; Samadi, M.; Yousefzadeh, S.; Soltani, M.; Rahimi, A.; Chou, T.-C.; Chen, L.-C.; Chen, K.-H.; Moshfegh, A. Z. Improved Solar-Driven Photocatalytic Activity of Hybrid Graphene Quantum Dots/ZnO Nanowires: A Direct Z-Scheme Mechanism. *ACS Sustainable Chemistry & Engineering* **2017**, *5* (1), 367–375.
139) Xu, F.; Chen, J.; Guo, L.; Lei, S.; Ni, Y. In situ electrochemically etching-derived

ZnO nanotube arrays for highly efficient and facilely recyclable photocatalyst. *Applied Surface Science* **2012**, *258* (20), 8160–8165.
140) Chu, D.; Masuda, Y.; Ohji, T.; Kato, K. Formation and Photocatalytic Application of ZnO Nanotubes Using Aqueous Solution. *Langmuir* **2010**, *26* (4), 2811–2815.
141) Wang, H.; Li, G.; Jia, L.; Wang, G.; Tang, C. Controllable Preferential-Etching Synthesis and Photocatalytic Activity of Porous ZnO Nanotubes. *The Journal of Physical Chemistry C* **2008**, *112* (31), 11738–11743.
142) Singh, R.; Verma, K.; Patyal, A.; Sharma, I.; Barman, P. B.; Sharma, D. Nanosheet and nanosphere morphology dominated photocatalytic & antibacterial properties of ZnO nanostructures. *Solid State Sciences* **2019**, *89*, 1–14.
143) Wang, M.; Zhang, Y.; Zhou, Y.; Yang, F.; Kim, E. J.; Hahn, S. H.; Seong, S. G. Rapid room-temperature synthesis of nanosheet-assembled ZnO mesocrystals with excellent photocatalytic activity. *CrystEngComm* **2013**, *15* (4), 754–763.
144) Di, J.; Xiong, J.; Li, H.; Liu, Z. Ultrathin 2D Photocatalysts: Electronic-Structure Tailoring, Hybridization, and Applications. *Advanced Materials* **2018**, *30* (1), 1704548–1704548.
145) Liu, D.; Lv, Y.; Zhang, M.; Liu, Y.; Zhu, Y.; Zong, R.; Zhu, Y. Defect-related photoluminescence and photocatalytic properties of porous ZnO nanosheets. *Journal of Materials Chemistry A* **2014**, *2* (37), 15377–15377.
146) Harish, S.; Archana, J.; Navaneethan, M.; Silambarasan, A.; Nisha, K. D.; Ponnusamy, S.; Muthamizhchelvan, C.; Ikeda, H.; Aswal, D. K.; Hayakawa, Y. Enhanced visible light induced photocatalytic activity on the degradation of organic pollutants by SnO nanoparticle decorated hierarchical ZnO nanostructures. *RSC Advances* **2016**, *6* (92), 89721–89731.
147) Galdámez-Martinez, A.; Santana, G.; Güell, F.; Martínez-Alanis, P. R.; Dutt, A. Photoluminescence of ZnO Nanowires: A Review. *Nanomaterials* **2020**, *10* (5), 857–857.
148) Wang, Y.; Li, X.; Wang, N.; Quan, X.; Chen, Y. Controllable synthesis of ZnO nanoflowers and their morphology-dependent photocatalytic activities. *Separation and Purification Technology* **2008**, *62* (3), 727–732.
149) Das, A.; Malakar, P.; Nair, R. G. Engineering of ZnO nanostructures for efficient solar photocatalysis. *Materials Letters* **2018**, *219*, 76–80.
150) Qu, Y.; Xu, X.; Huang, R.; Qi, W.; Su, R.; He, Z. Enhanced photocatalytic degradation of antibiotics in water over functionalized N,S-doped carbon quantum dots embedded ZnO nanoflowers under sunlight irradiation. *Chemical Engineering Journal* **2020**, *382*, 123016–123016.
151) Wang, T.; Centeno, A.; Darvill, D.; Pang, J. S.; Ryan, M. P.; Xie, F. Tuneable fluorescence enhancement of nanostructured ZnO arrays with controlled morphology. *Physical Chemistry Chemical Physics* **2018**, *20* (21), 14828–14834.
152) Wang, S.; Kuang, P.; Cheng, B.; Yu, J.; Jiang, C. ZnO hierarchical microsphere for enhanced photocatalytic activity. *Journal of Alloys and Compounds* **2018**, *741*, 622–632.
153) Yang, C.; Li, Q.; Tang, L.; Xin, K.; Bai, A.; Yu, Y. Synthesis, photocatalytic activity, and photogenerated hydroxyl radicals of monodisperse colloidal ZnO nanospheres. *Applied Surface Science* **2015**, *357*, 1928–1938.
154) Mirzaei, H.; Darroudi, M. J. C. I. Zinc oxide nanoparticles: Biological synthesis and biomedical applications. *Ceramics International* **2017**, *43* (1), 907–914.
155) Zhu, C.; Lu, B.; Su, Q.; Xie, E.; Lan, W. A simple method for the preparation of hollow ZnO nanospheres for use as a high performance photocatalyst. *Nanoscale* **2012**, *4* (10), 3060–3060.
156) Deng, Z.; Chen, M.; Gu, G.; Wu, L. A Facile Method to Fabricate ZnO Hollow Spheres and Their Photocatalytic Property. *The Journal of Physical Chemistry B* **2008**, *112* (1), 16–22.
157) Sheikh, M.; Pazirofteh, M.; Dehghani, M.; Asghari, M.; Rezakazemi, M.; Valderrama, C.; Cortina, J.-L. Application of ZnO nanostructures in ceramic and polymeric membranes for water and wastewater technologies: A review. *Chemical Engineering Journal* **2020**, *391*, 123475–123475.
158) Chiu, W. S.; Khiew, P. S.; Cloke, M.; Isa, D.; Tan, T. K.; Radiman, S.; Abd-Shukor, R.; Hamid, M. A. A.; Huang, N. M.; Lim, H. N. Photocatalytic study of two-dimensional ZnO nanopellets in the decomposition of methylene blue. *Chemical Engineering Journal* **2010**, *158* (2), 345–352.
159) Li, W.; Gao, S.; Li, L.; Jiao, S.; Li, H.; Wang, J.; Yu, Q.; Zhang, Y.; Wang, D.; Zhao, L. Hydrothermal synthesis of a 3D double-sided comb-like ZnO nanostructure and its growth mechanism analysis. *Chemical Communications* **2016**, *52* (53), 8231–8234.
160) Kim, S.; Kim, M.; Kim, T.; Baik, H.; Lee, K. Evolution of space-efficient and facet-specific ZnO 3-D nanostructures and their application in photocatalysis. *CrystEngComm* **2013**, *15* (14), 2601–2607.